JCB Journal of Cell Biology

ARTICLE

Target cell adhesion limits macrophage phagocytosis and promotes trogocytosis

Kirstin R. Rollins[1], Sareen Fiaz[1], Ishwaree Datta[1], and Meghan A. Morrissey[1]

Macrophage phagocytosis is an essential immune response that eliminates pathogens, antibody-opsonized cancer cells, and debris. Macrophages can also trogocytose, or nibble, targets. Trogocytosis and phagocytosis are often activated by the same signal, including IgG antibodies. What makes a macrophage trogocytose instead of phagocytose is not clear. Using both CD47 antibodies and a Her2 chimeric antigen receptor (CAR) to induce phagocytosis, we found that macrophages preferentially trogocytose adherent target cells instead of phagocytose in both 2D cell monolayers and 3D cancer spheroid models. Disrupting target cell integrin using an RGD peptide or through CRISPR-Cas9 knockout of the αV integrin subunit in target cells increased macrophage phagocytosis. In contrast, increasing cell–cell adhesion by ectopically expressing E-cadherin in Raji B cell targets reduced phagocytosis. Finally, we examined phagocytosis of mitotic cells, a naturally occurring example of cells with reduced adhesion. Arresting target cells in mitosis significantly increased phagocytosis. Together, our data show that adhesion of target cells limits phagocytosis and promotes trogocytosis.

Introduction

Macrophages are innate immune cells that surveil the body for signs of injury or infection. Macrophages clear diverse targets, including pathogens, dying cells, and debris, through phagocytosis (Freeman and Grinstein, 2021). Phagocytosis is critical for maintaining tissue homeostasis, protecting against infection, and preventing autoimmunity (Gordon, 2016). Macrophages are also key effectors of many cancer therapies (Guerriero, 2018; Van Wagoner et al., 2023; Weiskopf and Weissman, 2015). Therapeutic antibodies like rituximab (CD20 antibody) and trastuzumab (Her2 antibody) bind to cancer cells and signal for macrophage uptake (Chao et al., 2010; Gül et al., 2014; Manches et al., 2003; Shi et al., 2015; Uchida et al., 2004; Weiskopf and Weissman, 2015). IgG is recognized by the Fc receptor in macrophages (Nimmerjahn and Ravetch, 2008). Even many antibodies originally designed to block the function of their target benefit from activating the Fc receptor (Chen et al., 2019; Dahan et al., 2016). More recently, engineering macrophages to express synthetic chimeric antigen receptors (CARs) that trigger phagocytosis has been shown to shrink tumors in mouse models (Klichinsky et al., 2020; Morrissey et al., 2018; Sloas et al., 2021).

Activating phagocytosis of cancer cells is particularly exciting in solid tumors (Sloas et al., 2021). Macrophages are one of the most prevalent immune infiltrates of the solid tumor microenvironment (de Visser and Joyce, 2023). However, most studies on the mechanism of phagocytosis use suspended targets, including apoptotic cells, blood cancer cell lines, and reconstituted particles (Arandjelovic and Ravichandran, 2015; Gül et al., 2014; Joffe et al., 2020; Morrissey et al., 2018). Unlike these models, solid tumors have complex cell–cell and cell–ECM interactions that adhere cancer cells to the surrounding environment. How macrophages phagocytose a cell incorporated into a 3D tissue is not clear.

Phagocytosis of adherent targets often requires additional steps to remove the target from its environment. Adherent bacteria are pried from their substrate by a macrophage "hook-and-shovel" mechanism, wherein macrophages wedge lamellipodia between the bacteria and substrate to destroy adhesion molecules (Möller et al., 2013). Dying cells are loosened from their neighbors as focal adhesion and cell–cell contacts are dismantled during apoptosis (Brancolini et al., 1997). In melanoma models, macrophages cluster to cooperatively remove cancer cells (Dooling et al., 2023; Dooling et al., 2024, *Preprint*). These studies suggest that cell–cell and cell–substrate adhesion is a barrier to phagocytosis.

In addition to phagocytosis, macrophages can trogocytose, or nibble, target cells (Bettadapur et al., 2020). Trogocytosis has been observed in diverse contexts, including immune cell communication, developmental remodeling, and parasitic attack (Abdu et al., 2016; Gao et al., 2024; Hudrisier et al., 2001; Joly and Hudrisier, 2003; Mercer et al., 2018; Ralston et al., 2014; Weinhard et al., 2018). Trogocytosis and phagocytosis are triggered by the same signals, including IgG antibodies, and share

[1]Molecular Cellular and Developmental Biology Department, University of California, Santa Barbara, Santa Barbara, CA, USA.

Correspondence to Meghan A. Morrissey: morrissey@ucsb.edu.

© 2025 Rollins et al. This article is distributed under the terms as described at https://rupress.org/pages/terms102024/.

Check for updates

https://doi.org/10.1083/jcb.202502034

Downloaded from http://rupress.org/jcb/article-pdf/224/11/e202502034/1950889/jcb_202502034.pdf by guest on 12 May 2026

many molecular regulators (Bettadapur et al., 2020; Lindorfer and Taylor, 2022). What makes a macrophage trogocytose instead of phagocytose is not clear.

Macrophages also trogocytose antibody-opsonized cancer cells during cancer therapy (Beum et al., 2011; Lindorfer and Taylor, 2022; Park et al., 2022; Velmurugan et al., 2016). Trogocytosis of antibody-opsonized cancer cells can lead to cancer cell death (Finotti et al., 2023; Matlung et al., 2018; Velmurugan et al., 2016). However, trogocytosis is also associated with "antigen shaving," or the removal of target antigens, which limits antibody efficacy by making cancer cells more difficult for the immune system to detect (Beum et al., 2011; Hamieh et al., 2019; Kennedy et al., 2004; Williams et al., 2006). Biasing therapies toward phagocytosis could potentially improve cancer cell clearance (Greiner et al., 2025; Williams et al., 2006; Zent et al., 2014).

In this study, we investigated how adhesion of target cells impacts macrophage phagocytosis. We used an ovarian cancer cell line in 2D monolayers or 3D spheroids as a phagocytic target. Macrophages preferentially trogocytosed (nibbled) adherent cells and phagocytosed suspended cells. We show that this preference for trogocytosis was reversed if we reduced or eliminated cell–substrate adhesion. We also show that suspended cells were primarily trogocytosed instead of phagocytosed if we increased cell–cell adhesion. Finally, we observed that mitotic cells were more susceptible to phagocytosis than cells in interphase, indicating that macrophages may capitalize on opportune moments for phagocytosis upon the disassembly of adhesion. Together our results demonstrate that the macrophages preferentially trogocytose adherent targets.

Results

Construction of an Her2-targeting CAR

To study how macrophages attack adherent cells, we selected the SKOV3 ovarian cancer cell line as our target cell. This cell line has high expression of the human epidermal growth hormone receptor 2 (Her2/ErbB2). Trastuzumab, an antibody targeting Her2, is a common cancer therapy and has previously been shown to induce cancer cell internalization (Petricevic et al., 2013; Shi et al., 2015; Velmurugan et al., 2016). Her2-targeting CAR macrophages are being investigated in clinical trials (Klichinsky et al., 2020; Sloas et al., 2021).

We elected to induce phagocytosis with an Her2-targeted CAR, since Her2 antibodies inhibit Her2 signaling in addition to activating phagocytosis (Hudziak et al., 1989; Swain et al., 2023). We designed an Her2-targeting CAR comprised of an extracellular Her2 antibody fragment (scFv from 4D5-8 [Carter et al., 1992]), the CD8 hinge and transmembrane domain from successful CAR T molecules (Fesnak et al., 2016; Kochenderfer et al., 2009), the intracellular signaling domain from the mouse Fc receptor common gamma chain (Kern et al., 2021; Morrissey et al., 2018), and a GFP tag (Fig. 1 A). A similar Her2 CAR was recently shown to decrease cancer growth in mouse xenograft models lacking T cells, suggesting that Her2 CAR macrophages can shrink tumors without engaging the adaptive immune system (Klichinsky et al., 2020).

To test whether the Her2 CAR could stimulate macrophage activity, we added Her2$^+$ SKOV3 ovarian cancer cells dyed in Far Red CellTrace to Her2 CAR GFP or control GFP macrophages. After 3 h, we measured the cancer cell uptake via flow cytometry. We found that Her2 CAR expressing macrophages internalized significantly more SKOV3 cells than control GFP macrophages (Fig. 1 B). In contrast, Her2 CAR and control macrophages phagocytosed an equivalent number of Her2-negative apoptotic corpses (Fig. S1).

Her2 CAR macrophages primarily trogocytose target cells

To further characterize macrophage activity against adherent targets, we used confocal live-cell time-lapse imaging of Her2 CAR macrophages and SKOV3 co-incubations (Fig. S1). SKOV3 cells were infected with a membrane-tethered mCherry (mCherry-CAAX). To our surprise, phagocytosis of cancer cells was relatively rare. We observed that only 10% of macrophages phagocytosed during our 12-h time-lapse (Fig. 1 C and Video 1). In contrast, 95% of macrophages trogocytosed, or nibbled, the cancer cell membrane (Fig. 1 C and Video 2). These data show that most SKOV3 internalization is trogocytosis, rather than phagocytosis.

Her2 CAR macrophages limit the growth of SKOV3 spheroids

Our previous experiments in monolayers lacked the 3D architecture and cell–to–cell adhesion normally found in a solid tumor. To investigate macrophage eating dynamics in a simple 3D tissue model, we built spheroids of SKOV3 cells. To generate spheroids, we plated membrane-labeled (mCh-CAAX) SKOV3 cells in a low-adhesion dish in media supplemented with 2.5% Matrigel to favor cell–cell interactions (Ivascu and Kubbies, 2007; Heredia-Soto et al., 2018; Tofani et al., 2020). By 72 h, the SKOV3 cells assembled into consistent, compact spheroids (445 ± 65 µm in diameter). We then transferred the pre-assembled SKOV3 spheroids into a Matrigel dome containing Her2 CAR or control GFP macrophages. Z-stack images showed that both GFP and Her2 CAR macrophages could invade into the spheroids within 24 h (Videos 3 and 4). We tracked spheroid size for 10 days via spinning disc confocal imaging (Fig. 2, A and B). We found that Her2 CAR macrophages significantly reduced the size of the spheroids compared with no macrophages or GFP macrophages (Fig. 2 B, Fig. S2, and Data S1). In the final time points, a large portion of the remaining mCherry signal appeared to be from macrophages that had internalized cancer cells (Fig. 2 C). This demonstrates that Her2 CAR macrophages effectively attack 3D cancer spheroids.

Macrophages trogocytose more than phagocytose in a 3D environment

We next sought to determine if macrophages attack SKOV3 spheroids via trogocytosis as in the 2D culture system. Brief time-lapse imaging revealed several examples of trogocytosis and phagocytosis but was difficult to quantify (Video 5 and Fig. S2). Instead, we double-labeled cancer cells with a membrane tethered mCherry (mCh-CAAX) and a nuclear iRFP (H2B-iRFP; Fig. 2 D). If a cancer cell were phagocytosed, both nuclear and membrane signals would be detected within the macrophage,

Downloaded from http://rupress.org/jcb/article-pdf/224/11/e202502034/1950889/jcb_202502034.pdf by guest on 12 May 2026

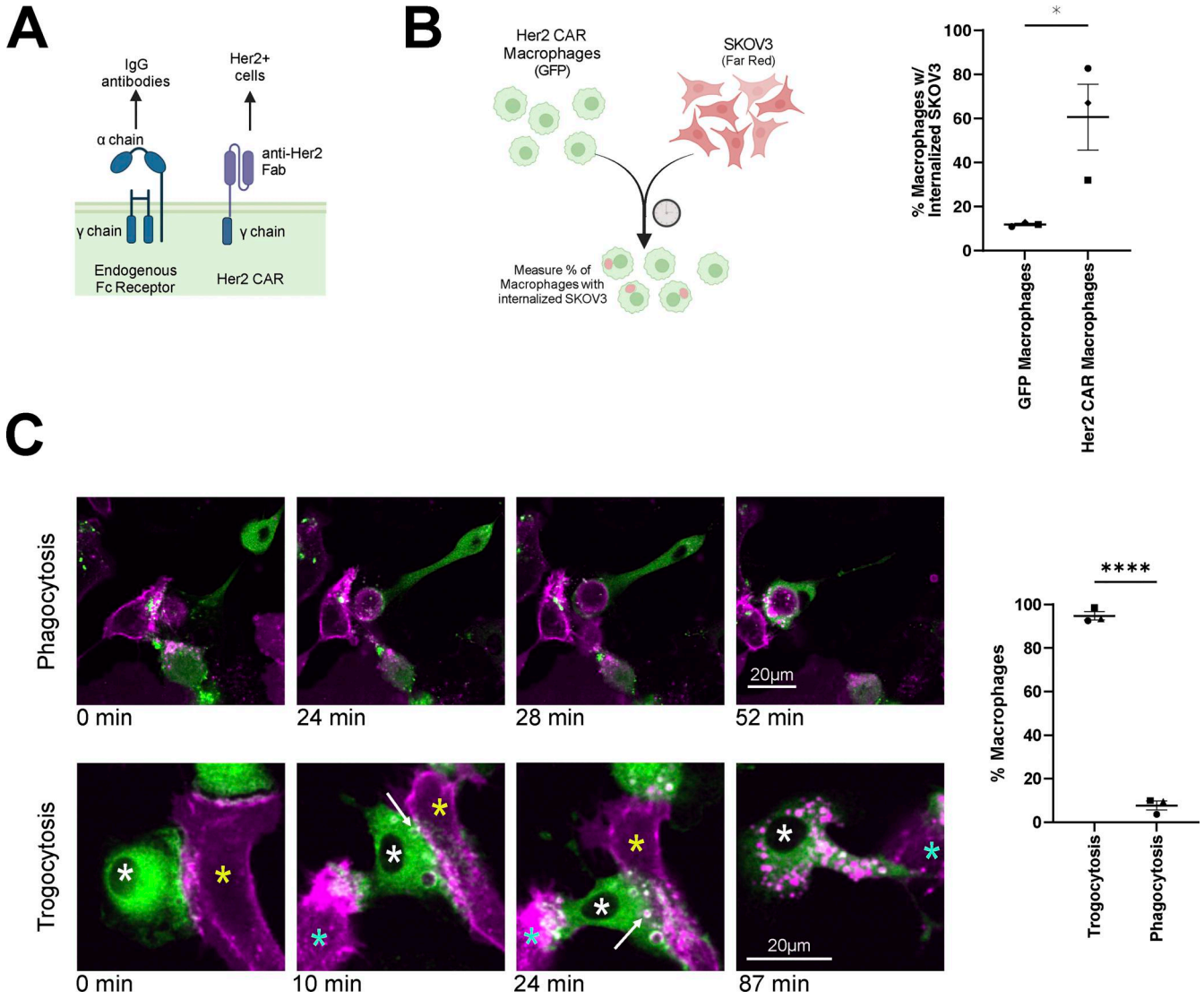

Figure 1. **Her2 CAR macrophages trogocytose target SKOV3 cells. (A)** Schematic shows the design of the Her2 CAR (right) compared with the native Fc receptor (left). The Her2 CAR contains an extracellular scFv recognizing Her2 and activates phagocytosis via the intracellular signaling domain from the endogenous Fc receptor common gamma chain. **(B)** Schematic (left) describes the assay quantified in the graph (right). SKOV3 cells dyed with CellTrace Far Red were added in suspension to adherent Her2 CAR GFP or control GFP (GFP-CAAX) bone marrow–derived macrophages (BMDMs). Flow cytometry was used to measure the percent of macrophages (GFP^+) that internalized cancer cell material ($Far\ Red^+$). **(C)** Her2 CAR GFP (green) macrophages were visualized interacting with SKOV3 cancer cells (mCh-CAAX; magenta) using time-lapse confocal microscopy. Stills from the images are depicted on the left, and the percent of macrophages engaging in trogocytosis (internalizing part of a cell) or phagocytosis (internalizing a whole cell) is graphed to the right. These stills correspond to Video 1 (top) and Video 2 (bottom). In B and C, data were compared using a two sided Student's *T* test. *N* = 3 experiments, consisting of ≥100 macrophages with independently generated and infected BMDMs. In all graphs, bars represent the mean ± SEM. Data collected on the same day are annotated with the same shape point. * denotes P < 0.05; **** denotes P < 0.0005. Scale bar denotes 20 μm.

confirming whole cell engulfment. If a cancer cell were trogocytosed, only the membrane signal would be detected within the macrophage. We imaged the spheroids daily for 10 days and quantified the fraction of macrophages that had internalized mCherry (trogocytosed) or iRFP and mCherry (phagocytosed) (Fig. 2, D and E). We found that trogocytosis was more common than phagocytosis in 3D spheroid models (Fig. 2 E), as in the 2D culture system. Trogocytic macrophages were clearly observed in the first days after macrophage infiltration, while phagocytic macrophages slowly accumulated over time (Fig. 2 E).

Macrophage trogocytosis strips the antigen from target cells

Trogocytosis may be a double-edged sword during cancer therapy. Neutrophils can kill antibody-opsonized cells via trogocytosis (Finotti et al., 2023; Matlung et al., 2018; Velmurugan et al., 2016). We tracked caspase activation in trogocytosed SKOV3 cells over time. While most SKOV3 cells were trogocytosed during our 12-h time-lapse, only 5–10% activated caspases (Fig. S3). This suggests that while some cells die after trogocytosis, many do not.

Several clinical studies have noted that trogocytosis of antibody-opsonized cancer cells removes target antigen from

Downloaded from http://rupress.org/jcb/article-pdf/224/11/e202502034/1950889/jcb_202502034.pdf by guest on 12 May 2026

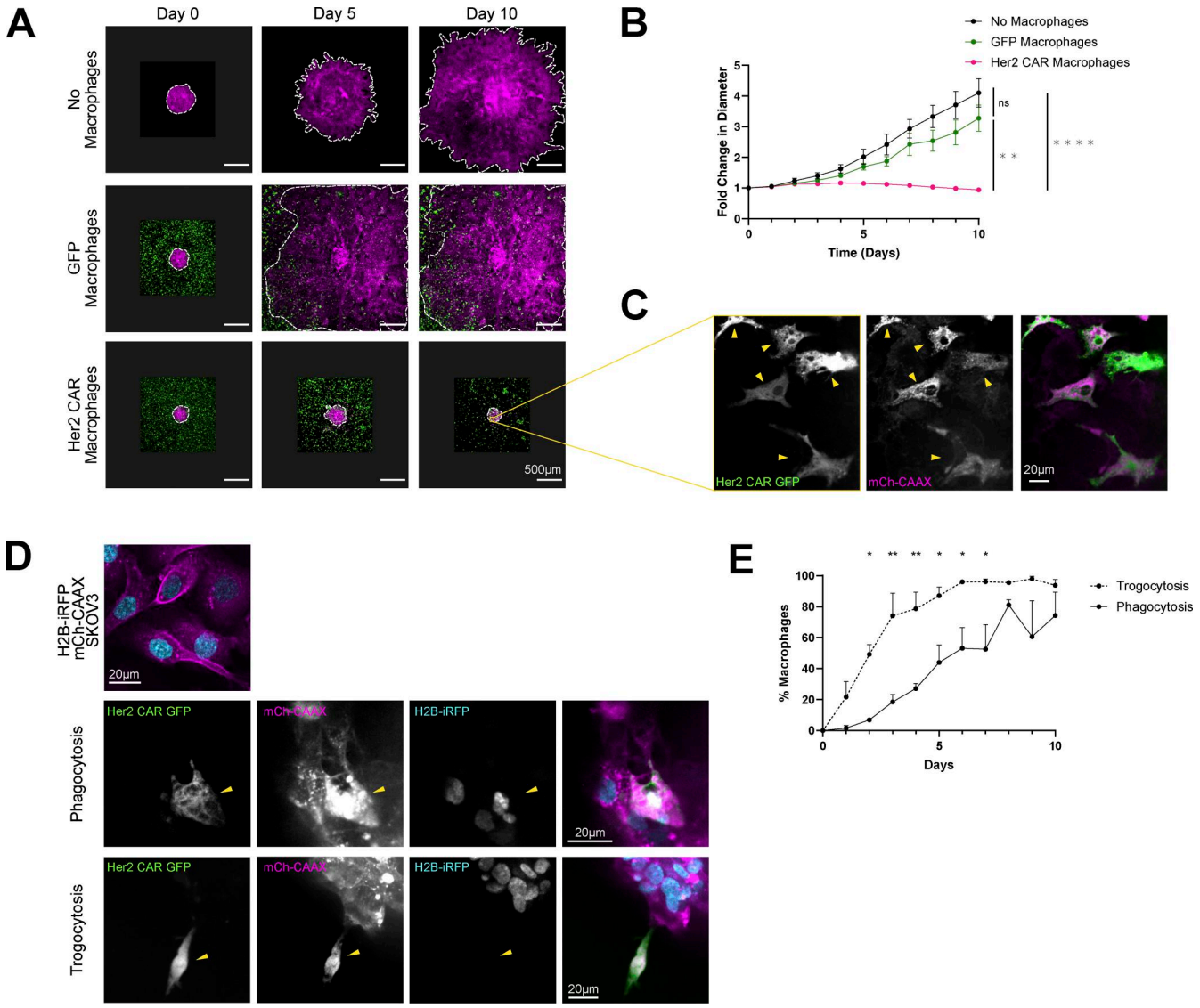

Figure 2. **Her2 CAR macrophages trogocytose more than phagocytose in 3D spheroid models. (A)** SKOV3 cells (mCh-CAAX, magenta) were assembled into a 3D spheroid and embedded in Matrigel alone (top), with control GFP (green) macrophages (middle), or with Her2 CAR GFP (green) macrophages (bottom). Images are maximum projections of spinning disc confocal z-stacks. Dashed line highlights the spheroid boundary. Scale bars denote 500 µm. On days 5 and 10, multiple images were stitched together to capture the entire spheroid in the no macrophage and GFP macrophage conditions. Unstitched images are presented on a gray background so the image scale is consistent. **(B)** Graph depicts spheroid growth over time for the same conditions shown in A. Individual spheroids were tracked for 10 days, and the diameter was normalized to the starting diameter. The length and width of the spheroid were measured on the max projection of confocal z-stacks and averaged to calculate spheroid diameter. *N* = 6 spheroids acquired in four independent experiments. The growth curves from individual spheroids in the Her2 CAR condition is shown in Fig. S2. **(C)** Inset from A shows that the mCherry signal on day 10 is mostly contained within Her2 CAR GFP (green) macrophages. Arrowheads point to macrophages. Scale bars denote 20 µm. **(D)** The top image shows the H2B-iRFP (blue), mCherry-CAAX (magenta) SKOV3 cell line used to assemble spheroids. Images show examples of Her2 CAR GFP (green) macrophages that have phagocytosed (middle, internalized nuclei position is highlighted with a yellow arrowhead) or trogocytosed (bottom, yellow arrowhead) SKOV3 cells. Scale bars denote 20 µm. **(E)** The percent of Her2 CAR GFP macrophages that had phagocytosed (internalized H2B-iRFP) or trogocytosed (internalized mCh-CAAX) was quantified on each day. Only macrophages touching the spheroid were included in the analysis. *N* = 3 spheroids from three independent experiments. In B, data acquired on day 10 were compared with a one-way ANOVA with Holm–Sidak multiple comparison test. In E, data from each day were compared with a two-way ANOVA. Bars represent the mean ± SEM. * denotes P < 0.05; ** denotes P < 0.005; **** denotes P < 0.00005.

the cancer cell surface in vivo (Hamieh et al., 2019; Lindorfer and Taylor, 2022; Park et al., 2022; Williams et al., 2006). This process, known as antigen shaving, makes the cancer cells more difficult for immune cells to detect (Hamieh et al., 2019; Lindorfer and Taylor, 2022; Williams et al., 2006). We observed that Her2 CAR macrophages co-incubated with SKOV3 cells had large puncta of internalized Her2 (Fig. 3 A). To quantify Her2 shaving on SKOV3 cells, we used flow cytometry to measure Her2 on SKOV3 cells after macrophage treatment. We found that treatment with Her2 CAR macrophages led to a substantial decrease in the surface levels of Her2, whereas GFP macrophages did not change Her2 surface levels (Fig. 3 B and

Downloaded from http://rupress.org/jcb/article-pdf/224/11/e202502034/1950889/jcb_202502034.pdf by guest on 12 May 2026

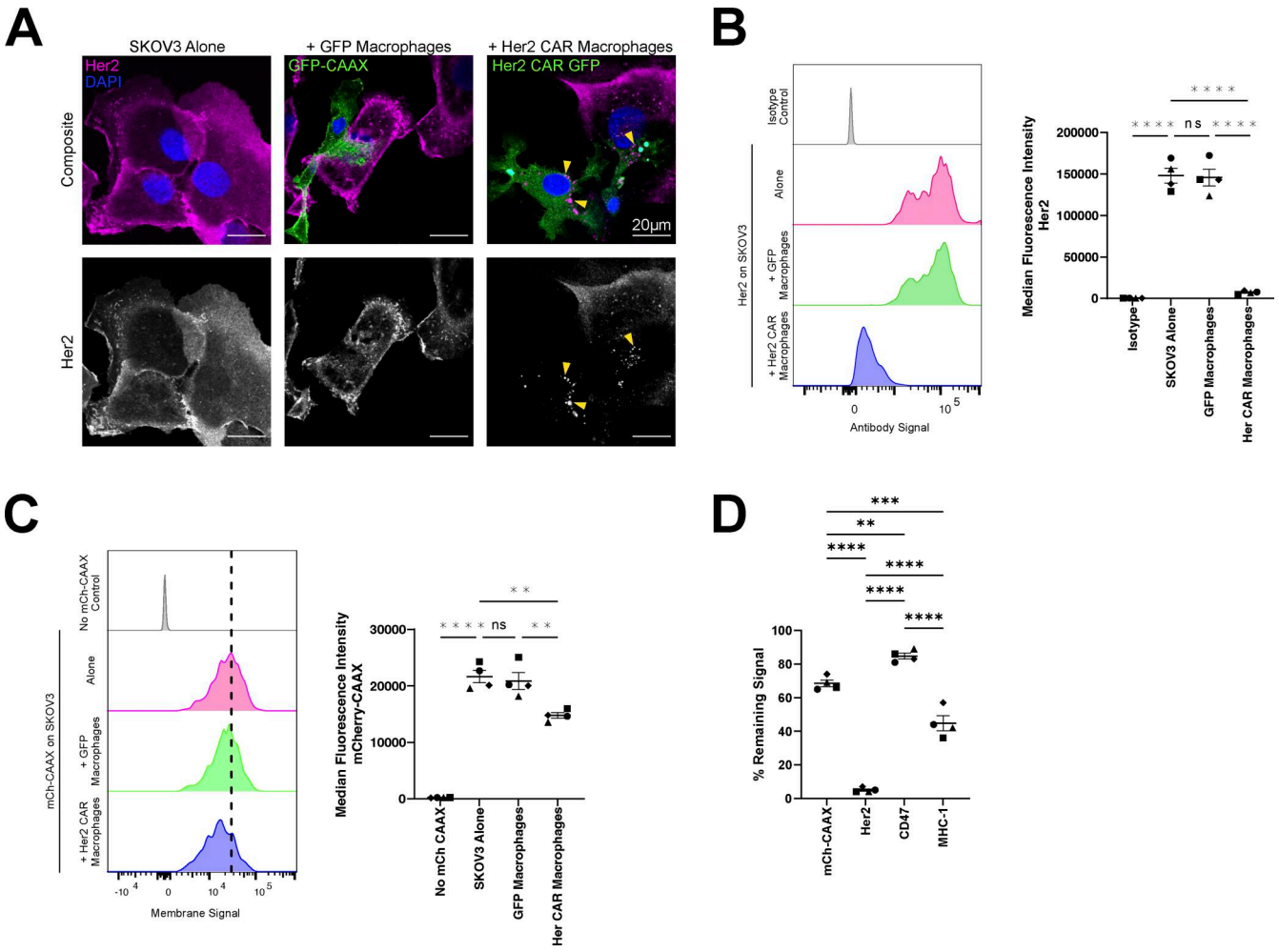

Figure 3. **Trogocytosis strips Her2 from SKOV3 target cells. (A)** Her2 CAR GFP or control GFP macrophages (GFP; green) were incubated with SKOV3 cells for 2 h. The cells were then stained for Her2 (magenta) and DAPI (blue). Her2 CAR macrophages showed bright puncta of internalized Her2 (yellow arrowhead). **(B)** For quantitative analysis of Her2 surface levels, Her2 CAR GFP or control GFP macrophages were incubated with SKOV3 cells (mCh-CAAX) for 2 h. The cells were then stained for Her2 and analyzed by flow cytometry. A representative flow histogram shows the Her2 levels on SKOV3 cells alone (pink) and SKOV3 cells incubated with Her2 CAR (blue) or control GFP macrophages (green). SKOV3 cells were also stained with an isotype control antibody as a negative control (gray). The graph depicts median fluorescence intensity of Her2. **(C)** Removal of a generic membrane tethered protein, mCh-CAAX, was quantified on the same SKOV3 cells. The graph depicts median fluorescence intensity of mCh-CAAX. **(D)** MHC-1 (HLA A–C) and CD47 removal was measured by antibody staining followed by flow cytometry. The percent remaining signal for Her2, MHC-1, and CD47 was calculated by dividing the signal in SKOV3 cells incubated with Her2 CAR macrophages by the signal in SKOV3 alone. Graphs B–D show data from $N = 4$ independent replicates. Bars represent the mean ± SEM of the replicates. Data were compared using a one way ANOVA with a Holm–Sidak multiple comparison test. Data collected on the same day are annotated with the same shape point. ** denotes $P < 0.005$; **** denotes $P < 0.0005$. Scale bar denotes 20 μm.

Fig. S3). In contrast to Her2, membrane-tethered mCherry (mCherry-CAAX) was only slightly reduced on trogocytosed cells (Fig. 3 C). As a control, we measured depletion of two other membrane proteins, CD47 and MHC-1 (Fig. 3 D). Her2 was much more depleted than CD47 or MHC-1. Overall, these data show striking depletion of Her2 from target cells.

Macrophages primarily phagocytose suspended cells and trogocytose adherent cells

Prior studies using antibody-opsonized B cells have reported high levels of phagocytosis (for example [Chao et al., 2010; Gül et al., 2014]). We have previously seen that CD19 CAR macrophages targeting B cells phagocytose many cancer cells during a similar time-lapse microscopy experiment (Mishra et al., 2023; Morrissey et al., 2018). We hypothesized that adherent cells may be more difficult to phagocytose and more likely to be trogocytosed than suspended cells. To see if this was broadly true for multiple adherent cell lines, we assembled a panel of cancer cell lines, including three adherent cell lines and two suspension cell lines (Fig. 4 A). We opsonized with a CD47 antibody, as all of the selected cancer cell lines expressed a reasonably uniform level of CD47, a "Don't Eat Me" signal (Fig. 4 B). CD47 antibodies trigger phagocytosis by blocking the inhibitory CD47 signal and engaging with macrophage Fc receptors through the antibody Fc domain (Chao et al., 2010; Jaiswal et al., 2009; Majeti et al., 2009; Osorio et al., 2023). We expressed membrane-tethered mCherry-CAAX and a nuclear H2B-iRFP marker in all the cell lines, opsonized the cells with a CD47 antibody, and measured

Downloaded from http://rupress.org/jcb/article-pdf/224/11/e202502034/1950889/jcb_202502034.pdf by guest on 12 May 2026

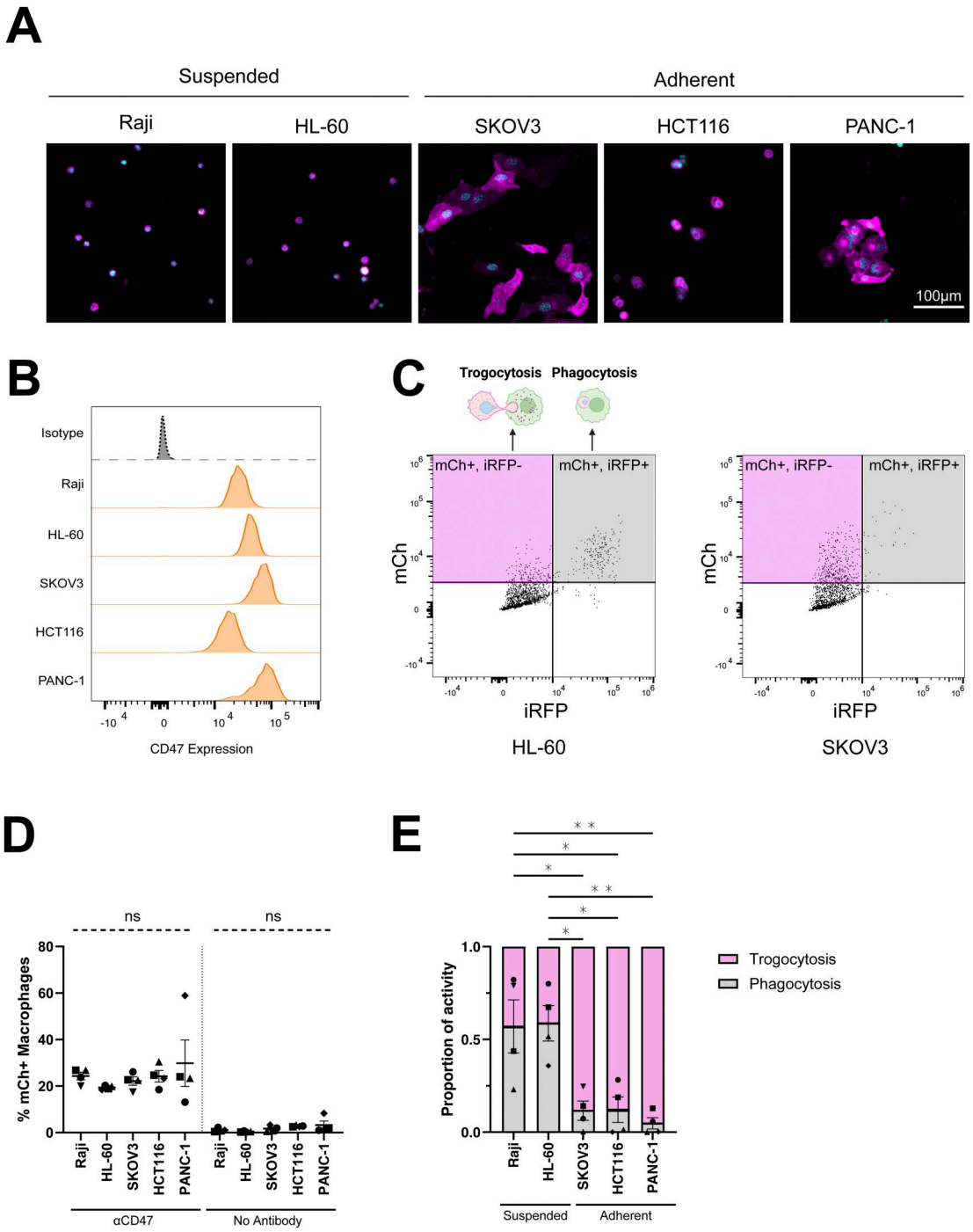

Figure 4. **Trogocytosis is more common than phagocytosis in multiple adherent cancer cell lines.** Cancer cells were opsonized with a mouse anti-human CD47 antibody, and the amount of phagocytosis and trogocytosis was measured by flow cytometry. **(A)** Images show the double labeled (mCh-CAAX, H2B-iRFP) cancer cells used to distinguish phagocytosis and trogocytosis. **(B)** The cancer cell lines used were stained with a CD47 antibody and analyzed by flow cytometry. CD47 antibody binding was compared with an isotype control (gray). **(C)** Representative flow plots show the assay for distinguishing phagocytosis and trogocytosis by flow cytometry. **(D)** Graph shows the percent of mCherry-positive macrophages, indicating that these macrophages internalized some cancer cell material. **(E)** The graph shows the fraction of mCherry-positive macrophages that were also positive for iRFP, indicating cancer cell phagocytosis (gray), or lacking iRFP, indicating trogocytosis (pink). For D and E, data were compared using one-way ANOVA with Holm–Sidak multiple comparison correction. *N* = 4 independent experiments, consisting of three averaged technical replicates. Bars represent the mean ± SEM. Data collected on the same day are annotated with the same shape point. * denotes P < 0.05; ** denotes P < 0.005. Scale bar denotes 100 µm.

Downloaded from http://rupress.org/jcb/article-pdf/224/11/e202502034/1950889/jcb_202502034.pdf by guest on 12 May 2026

trogocytosis and phagocytosis with flow cytometry (Fig. 4 C). We found that the total number of macrophages internalizing any cancer cell material (mCherry positive) was relatively uniform across the 5 cell lines (Fig. 4 D). Strikingly, we observed that the suspended cell lines were primarily phagocytosed (60–70% of total activity) and the adherent cell lines were primarily trogocytosed (80–90% of total activity; Fig. 4 E). Since antibody opsonization induced trogocytosis of multiple adherent cell lines, this demonstrates that trogocytosis is not a unique feature of the SKOV3 target cell or of the CAR macrophage system.

Decreasing target cell adhesion increases phagocytosis

We hypothesized that decreasing adhesion of target cells could shift macrophage behavior from trogocytosis to phagocytosis. First, we tested if detaching SKOV3 cells from a substrate increased phagocytosis. We compared phagocytosis of adherent SKOV3 cells with phagocytosis of detached SKOV3 cells (Fig. 5 A). Using time-lapse microscopy to measure phagocytosis, we found Her2 CAR macrophages phagocytosed more SKOV3 cells when the cells were presented in suspension than when allowed to adhere to a tissue culture plate (Fig. 5 B and Fig. S4). This was true whether the macrophages were mixed with the SKOV3 cells in suspension or pre-adhered to the tissue culture plate (Fig. S4). Control GFP macrophages did not phagocytose more suspended cells, suggesting this increase in phagocytosis was due to Her2 CAR activity, not increased cell death (Fig. 5 B). Together, these data show that suspended cells are more readily phagocytosed than adherent cells.

We next sought to modulate cell–substrate attachment by decreasing integrin adhesion. To weaken cell–substrate adhesion, we treated SKOV3 cells expressing membrane-tethered mCherry and nuclear iRFP with the RGD peptide, cilengitide trifluoroacetate. This RGD peptide primarily inhibits the integrins $\alpha_V\beta_3$ and $\alpha_v\beta_5$ (Dechantsreiter et al., 1999). We verified that the RGD peptide caused the SKOV3 cells to adopt a rounded morphology and decreased surface area characteristic of lowered adhesion, although the cells were not completely suspended (Fig. 5 A). To minimize the RGD peptide's effect on the macrophages, we washed out the RGD peptide before adding Her2 CAR or control GFP macrophages. We then measured phagocytosis and trogocytosis by live-cell time-lapse microscopy. We found that RGD peptide promoted phagocytosis and reduced trogocytosis, although fewer cells were phagocytosed than when the SKOV3 cells were fully detached from the substrate (Fig. 5 B). Again, control GFP macrophages did not phagocytose additional target cells in the RGD condition, suggesting that these cells are not exposing additional pro-phagocytic signals. We repeated this experiment using the CD47 antibody to induce phagocytosis instead of the Her2 CAR. We found that treating antibody-opsonized SKOV3 cells with RGD peptide increased phagocytosis (Fig. 5 C). This suggests that inhibiting integrin is sufficient to increase phagocytosis.

To confirm that inhibiting integrin in the target cell increases phagocytosis, we used CRISPR-Cas9 to knock out specific integrin subunits in SKOV3 cells (Fig. S4 and Table S1). We selected integrin β1 and β5 (ITGB1 and ITGB5) as dysregulation of these receptors is associated with cancer development and progression in a wide variety of solid tumors, including Her2$^+$ breast and ovarian cancers (Casey et al., 2001; Davidson et al., 2003; Desgrosellier and Cheresh, 2010). We also selected integrin αV (ITGAV), as it is reported to affect ovarian cancer proliferation and metastasis (Casey et al., 2001; Cruet-Hennequart et al., 2003; Davidson et al., 2003). ITGAV knockout SKOV3 cells showed significantly reduced focal adhesions, while ITGB1 and ITGB5 knockouts had little impact on focal adhesion area or number (Fig. 5, D and E). ITGAV knockout target cells were phagocytosed more than control cells (Fig. 5 F). ITGB1 and ITGB5 knockouts did not significantly impact phagocytosis, consistent with the limited impact on focal adhesions. This could indicate redundancy since ITGAV pairs with both B subunits. These findings demonstrate decreasing cell–substrate adhesion promotes phagocytosis.

Increasing cell–cell adhesion in suspension cells decreases phagocytosis

We next wondered if we could conversely increase adhesion to limit phagocytosis. We postulated that any adhesion system would mechanically limit phagocytosis by increasing the force macrophages must exert to internalize a target cell. To test this, we overexpressed E-cadherin (CDH1) in Raji B cells, a suspension cell line. Raji B cells expressing E-cadherin formed multicellular clusters, indicating increased cell–cell adhesion (Fig. 6 A). We opsonized wild-type and E-cadherin–overexpressing Rajis with a mouse anti-human CD47 antibody to induce phagocytosis. Macrophages with Rajis expressing either iRFP-CAAX or H2B-iRFP were co-incubated for 2 h before dissociating the clustered conditions into a single-cell solution for flow cytometry. The level of phagocytosis (H2B-iRFP internalization) was significantly lower in the E-cadherin–overexpressing clusters than in the wild-type Raji cells (Fig. 6 B). In contrast, the fraction of macrophages with internalized Raji cell membrane (iRFP-CAAX), either by trogocytosis or phagocytosis, did not change (Fig. 6 C). This suggests that macrophages encountered a similar number of Raji targets but did not phagocytose the E-cadherin–overexpressing cells. Overall, this demonstrates that increasing cell–cell adhesion in target cells limits phagocytosis.

Dividing cells are more vulnerable to phagocytic attack

Our data demonstrate that macrophages phagocytose cellular targets with weakened attachment to substrates and neighboring cells. However, even without any synthetic manipulations of target cell adhesion, we observed that 10% of macrophages could phagocytose adherent SKOV3 cells (Fig. 1 C). We revisited these intrinsic phagocytic attacks in our time-lapses and found that a large number of the phagocytosed cells appeared to be in the process of cell division (Fig. 7 A and Video 6). While only 4% of SKOV3 cells were dividing at any time, 38% of the phagocytosed SKOV3 cells were undergoing division (Fig. 7 B). Mitotic cells are known to have reduced adhesion (Akhmanova et al., 2022; Dix et al., 2018; Lock et al., 2018; Marchesi et al., 2014), so this observation is consistent with our overall hypothesis that reduced cell adhesion promotes phagocytosis.

To examine this more closely, we generated an SKOV3 cell line expressing fluorescent ubiquitination-based cell cycle

Downloaded from http://rupress.org/jcb/article-pdf/224/11/e202502034/1950889/jcb_202502034.pdf by guest on 12 May 2026

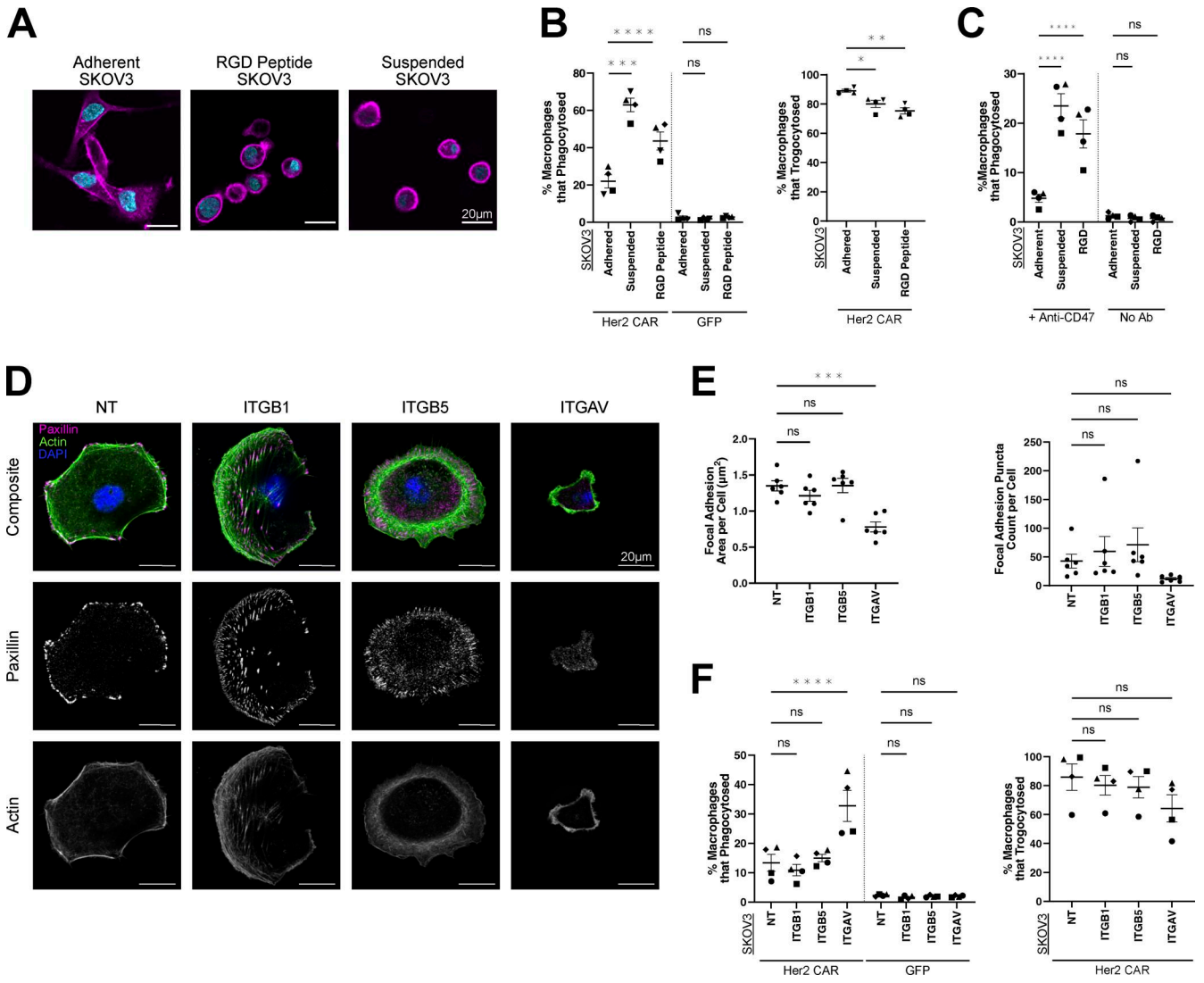

Figure 5. **Reducing cancer cell adhesion promotes phagocytosis. (A)** SKOV3 cells with a membrane tethered mCherry (mCh-CAAX) and a nuclear iRFP (H2B-iRFP) were plated untreated 8 h prior (adherent), with 50 µg/ml RGD peptide 8 h prior (RGD Peptide), or untreated at the time of macrophage addition (suspended). **(B)** Her2 CAR GFP or control GFP-CAAX macrophages were incubated with adherent SKOV3 cells, RGD peptide–treated SKOV3 cells, or suspended SKOV3 cells. The percent of macrophages that phagocytosed (right) and trogocytosed (left) was measured during an 8-h time-lapse. **(C)** The same experimental conditions were recapitulated with GFP-CAAX macrophages in either the presence or absence of opsonization with anti-CD47. **(D)** SKOV3 were infected with CRISPR-Cas9 and an sgRNA-targeting integrin β1, β5, αV, or a NT control guide. Infected cells were selected with puromycin. Knockout cells lines were stained for paxillin (magenta) and phalloidin (actin, green) to validate change in the amount of focal adhesions and structural morphology. Nuclei were labeled with DAPI (blue). **(E)** Paxillin was used to determine the total area of focal adhesion per cell (left) and the total count of focal adhesions per cell (right) in the knockout lines. **(F)** SKOV3 cells expressing mCherry-CAAX and H2B-iRFP were infected with the same CRISPR-Cas9 and sgRNA. Infected cells were selected with puromycin, and knockdown was confirmed by flow cytometry (Fig. S4). The resulting polyclonal cell lines were incubated with Her2 CAR GFP or control GFP-CAAX macrophages, and the percent of macrophages that phagocytosed (left) and trogocytosed (right) was measured during an 8-h time-lapse. Data in E and F were compared using one-way ANOVA with Holm–Sidak multiple comparison correction. *N* = 4 independent experiments in B, C, and F, *N* = 6 in E. For B, C, E, and F, bars represent the mean ± SEM. Data collected on the same day are annotated with the same shape point. * denotes P < 0.05; ** denotes P < 0.005; *** denotes P < 0.0005; **** denotes P < 0.00005. Scale bars denote 20 µm.

indicator (FUCCI) to read out the stage of the cell cycle. The FUCCI reporter consists of an mCherry-tagged hGeminin that will accumulate in S/G2/M before being degraded, and a BFP-tagged hCdt1 will be detected in G1 (Fig. 7 C) (Sakaue-Sawano et al., 2008; Sato et al., 2019). Using this reporter, we found that 94% of phagocytosed SKOV3 were mCherry positive, indicating that these cells were in S/G2/M, while only 53% of the overall SKOV3 population was mCherry positive (Fig. 7 D). This is consistent with our observation that SKOV3 cells are more likely to be phagocytosed while dividing.

We next hypothesized that arresting target cells in mitosis would increase phagocytosis. To test this, we treated cancer cells with paclitaxel or S-trityl-cysteine (STLC). Paclitaxel is a cancer chemotherapeutic that inhibits microtubule disassembly and prevents cells from passing the spindle assembly checkpoint (Horwitz, 1994). STLC inhibits Eg5, a mitotic kinesin necessary

Downloaded from http://rupress.org/jcb/article-pdf/224/11/e202502034/1950889/jcb_202502034.pdf by guest on 12 May 2026

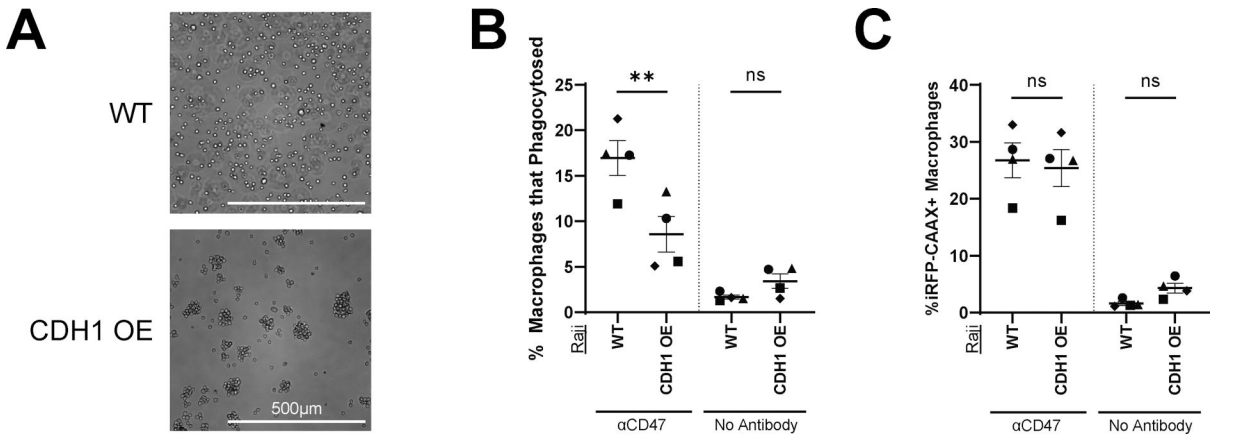

Figure 6. **Increasing cancer cell adhesion reduces cancer cell phagocytosis. (A)** Raji B cells were infected with E-cadherin GFP (CDH1 OE) to induce cell–cell adhesion. Bright-field images show the formation of cell clusters in CDH1-overexpressing cells. **(B)** Raji B cells expressing H2B-iRFP were opsonized with a CD47 antibody and incubated with mCh-CAAX macrophages for 2 h. The percent of phagocytic macrophages was measured by flow cytometry. Scale bars denote 500 µm. **(C)** Raji B cells expressing iRFP-CAAX were opsonized with a CD47 antibody and incubated with mCh-CAAX macrophages for 2 h. The percent of iRFP-positive macrophages was measured by flow cytometry. Data were compared using one-way ANOVA with Holm–Sidak multiple comparison correction. *N* = 4 independent experiments. Bars represent the mean ± SEM. Data collected on the same day are annotated with the same shape point. ** denotes $P < 0.005$.

for assembly of the bipolar spindle, locking the cells in prometaphase (Skoufias et al., 2006). After 20 h of paclitaxel and STLC treatment, nearly all FUCCI SKOV3 cells were mCherry positive, indicating cell cycle arrest (Fig. 7, C and D). The mitotic arrest did not induce apoptosis by 20 h, as we did not detect an increase in phosphatidylserine exposure (Fig. S5 A). We then co-incubated the arrested cells with Her2 CAR macrophages and measured phagocytosis by time-lapse microscopy. We found that cancer cells arrested in mitosis were phagocytosed significantly more than untreated controls (Fig. 7 E). These data suggest that mitotic SKOV3 cells are easier to phagocytose than interphase cells.

We hypothesized that suspended cells would not be more vulnerable to phagocytosis during cell division, since they lack focal adhesions to disassemble. To test this, we arrested Raji B cells in mitosis using paclitaxel and STLC. To activate phagocytosis, we opsonized paclitaxel-treated, STLC-treated, and control cells with a CD47 antibody. Arrested Raji B cells were phagocytosed to a similar extent as control cells (Fig. 7 F).

Discussion

While many antibody therapies and CAR macrophages are presumed to primarily trigger phagocytosis, we have found that phagocytosis of adherent cells is relatively rare. Instead, macrophages trogocytose, or nibble, these cells. Reducing adhesion of target cells by disrupting integrin increased macrophage phagocytosis and reduced trogocytosis. Conversely, increasing cell–cell adhesion in a suspended cell line reduced phagocytosis. Overall, these data show that target cell adhesion regulates phagocytosis and trogocytosis.

Very little is known about what makes a macrophage trogocytose instead of phagocytose. Trogocytosis and phagocytosis are controlled by nearly identical signaling pathways in the macrophage (Bettadapur et al., 2020). Trogocytosis and phagocytosis also occur on diverse targets, making it unlikely that there is a specific molecule that signals for trogocytosis instead of phagocytosis (Bettadapur et al., 2020). Instead, the biophysical properties of the target cell may guide the macrophage to trogocytose instead of phagocytose. A recent study found that decreased target membrane tension promotes trogocytosis (Cornell et al., 2024, *Preprint*). Conversely, increasing target stiffness promotes phagocytosis (Beningo and Wang, 2002; Settle et al., 2024). Our study also supports the hypothesis that the target's biophysical properties determine if a macrophage performs phagocytosis or trogocytosis.

Trogocytosis has been observed in many clinical settings (Hamieh et al., 2019; Lindorfer and Taylor, 2022; Park et al., 2022; Suzuki et al., 2015; Williams et al., 2006). The impact of trogocytosis is murky. Sometimes, trogocytosis kills the target cell (Finotti et al., 2023; Matlung et al., 2018; Park et al., 2022; Velmurugan et al., 2016). In other cases, trogocytosis limits the efficacy of cancer therapy. Trogocytosis of the CD20 antibody therapy rituximab causes a significant reduction in CD20 levels on cancer cells in rituximab-treated patients (Kennedy et al., 2004). Optimizing the rituximab dosing schedule to limit trogocytosis improved efficacy (Williams et al., 2006; Zent et al., 2014). Similarly, high-affinity CAR T cells trogocytose target antigen from the cancer cell's surface, leading to antigen escape (Hamieh et al., 2019). Reengineering the CAR T molecule to have a lower affinity increased efficacy by reducing antigen shaving. These studies suggest that biasing antibody therapies toward phagocytosis instead of trogocytosis could significantly reduce antigen shaving and improve clinical efficacy. Importantly, these studies also highlight that trogocytosis of antibody-opsonized cancer cells occurs in a clinical setting not just the ex vivo models used in this study. Future studies imaging CAR macrophage trogocytosis in vivo could significantly add to our understanding of this process.

Downloaded from http://rupress.org/jcb/article-pdf/224/11/e202502034/1950889/jcb_202502034.pdf by guest on 12 May 2026

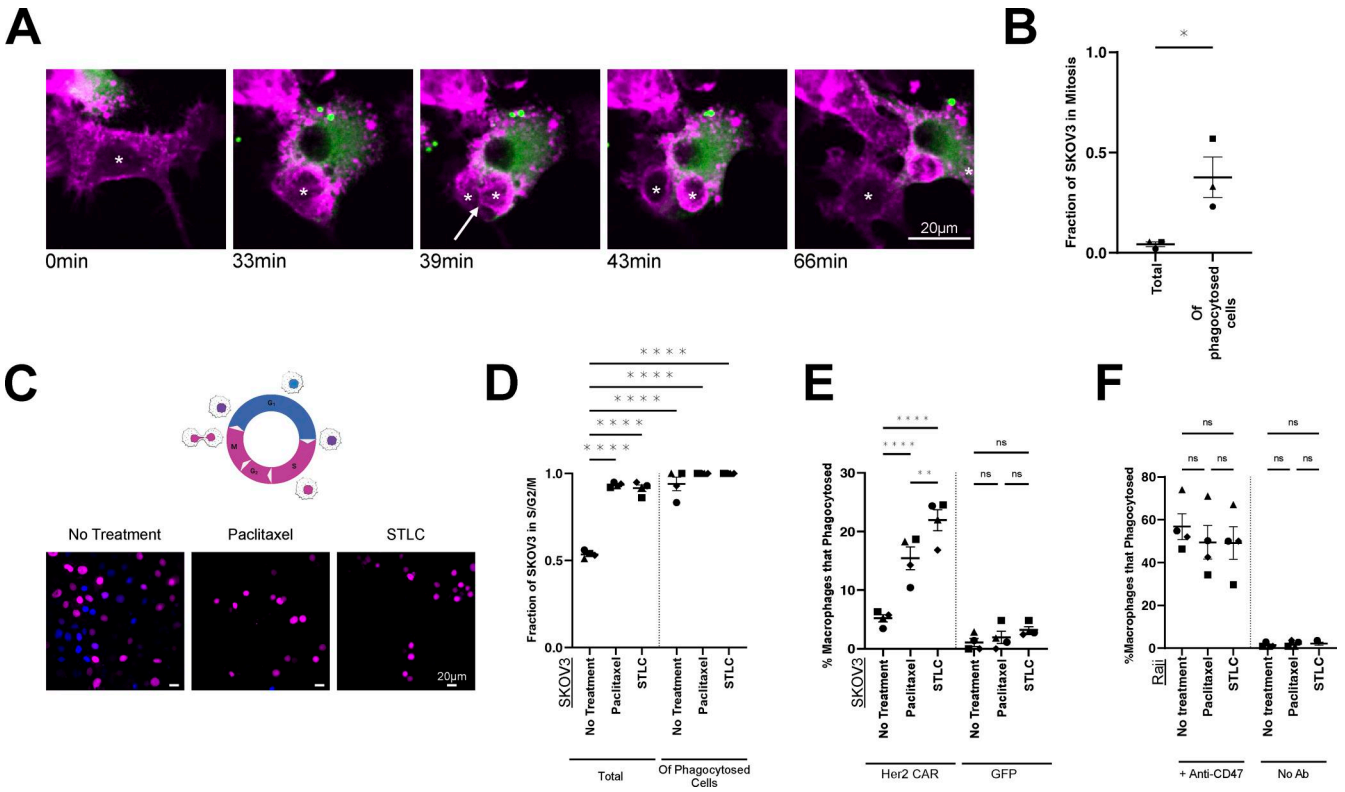

Figure 7. **Mitotic cells are phagocytosed more than their interphase neighbors. (A)** Stills from Video 6 show an Her2 CAR GFP (green) macrophage phagocytosing a mitotic SKOV3 (mCherry-CAAX, magenta). **(B)** The graph shows the fraction of SKOV3 undergoing division in the entire population (left) compared with the fraction of phagocytosed SKOV3 cells undergoing division (right). **(C)** SKOV3 cells expressing FUCCI were treated with 0.1 μM paclitaxel or 1 μM STLC for 20 h to arrest cells in mitosis. Image shows cells in G1 phase (blue; hCdt1) and S/G2/M (magenta; hGeminin). **(D)** SKOV3 cells were treated with paclitaxel or STLC for 20 h, then the inhibitors were removed and replaced with fresh media and Her2 CAR GFP macrophages. The fraction of mCherry+ FUCCI SKOV3 cells (indicating S/G2/M phase) was measured for the entire SKOV3 population (total) and for the SKOV3 cells that were phagocytosed (of phagocytosed cells) during a 4-h time-lapse. **(E)** The graph shows the percent of Her2 CAR GFP or GFP-CAAX macrophages phagocytosing a cancer cell in the same experiment. **(F)** Raji B cells were treated with 0.1 μM paclitaxel or 1 μM STLC for 20 h to arrest cells in mitosis. The graph shows the percent of GFP-CAAX macrophages phagocytosing Raji cells opsonized with anti-CD47 antibody or with no antibody. For B, data were compared using a two sided Student's *T* test and *N* = 3 independent experiments, consisting of ≥100 macrophages per replicate. For D–F, data were compared using one-way ANOVA with Holm–Sidak multiple comparison correction. *N* = 4 independent experiments, consisting of ≥100 macrophages per replicate. Bars represent the mean ± SEM. Data collected on the same day are annotated with the same shape point. * denotes P < 0.05; ** denotes P < 0.005; **** denotes P < 0.00005. Scale bars denote 20 μm.

What determines if cancer cells die after trogocytosis is unclear. We found that the majority of SKOV3 cells co-cultured with Her2 CAR macrophages showed significant shaving of the Her2 antigen, while only a small portion of the SKOV3 cells were apoptotic. Despite the relatively low levels of phagocytosis and apoptosis, Her2 CAR macrophages were able to shrink SKOV3 spheroids over several days. We postulate that while most target cells survive trogocytosis, some undergo apoptosis or necrosis after trogocytosis. In combination with the low levels of phagocytosis, this may be sufficient to shrink spheroids. Whether target cells survive or die might be stochastic or depend on cancer cells effectively using membrane repair or cell survival pathways (van Rees et al., 2022). Sustained trogocytosis over several days, as in the spheroids, may also lead to cumulative damage that kills the target cells over time. Future studies will need to dissect what determines if trogocytosis kills target cells or simply strips off antigen. This is especially important given that the first phase 1 clinical trial for CAR macrophages showed favorable safety, but the best overall response was stable disease (Reiss et al., 2025). This study used macrophages expressing an Her2 CAR similar to our molecule, but using the intracellular signaling domain of the T cell receptor instead of the native Fc receptor. Optimizing CAR macrophages to prefer phagocytosis over trogocytosis, or increasing the lethality of trogocytosis could significantly improve this therapy (Greiner et al., 2025; Mishra et al., 2023).

We found that arresting cancer cells in mitosis increased CAR macrophage phagocytosis. Dividing cells disassemble focal adhesion while remaining loosely attached to their underlying substrate (Dix et al., 2018). This lowered adhesion allows macrophages to squeeze past dividing cells and infiltrate cell-dense tissue (Akhmanova et al., 2022). Dividing cells undergo other cell shape changes that may promote phagocytosis, including cell rounding. However, given our data showing that decreasing cell adhesion promotes phagocytosis, we attribute at least part of the increased phagocytosis to decreased cell adhesion. Interestingly, a combination of paclitaxel and Her2 mAb is a highly effective treatment for Her2-positive breast cancers (Giordano et al., 2022). This suggests that the current therapy regimen could already benefit from enhanced phagocytosis due

Downloaded from http://rupress.org/jcb/article-pdf/224/11/e202502034/1950889/jcb_202502034.pdf by guest on 12 May 2026

to mitotic arrest. Future studies will need to test if this is also an effective combination for CAR macrophage therapies.

We also demonstrate that reducing integrin-mediated adhesion in target cells increased macrophage phagocytosis. Integrin inhibitors have previously been targeted in several clinical trials (Desgrosellier and Cheresh, 2010). Unfortunately, many of these integrin inhibitors failed in clinical trials due to lack of efficacy. Our work suggests that while these inhibitors were ineffective as a monotherapy, they may synergize with antibody therapies or CAR macrophages that induce phagocytosis.

Macrophages cooperate to phagocytose in solid tumor models (Dooling et al., 2023; Dooling et al., 2024, *Preprint*). Our studies support the idea that cell–cell and cell–matrix adhesions are too strong for a single macrophage to overcome during phagocytosis (Dooling et al., 2023). We speculate that trogocytosis could be a mechanism for macrophage cooperation by weakening target cells. Our data show higher occurrence of trogocytosis than phagocytosis in the initial days after macrophages infiltrate the spheroid. The subsequent increase in phagocytosis is consistent with cancer cells dying due to trogocytosis, then their corpses being phagocytosed, or with trogocytosis enabling phagocytosis. Currently, there are no tools to specifically block trogocytosis without impacting phagocytosis as well, since the molecules involved in trogocytosis appear to also be required for phagocytosis. Future studies will need to test how trogocytosis impacts phagocytosis and antibody efficacy.

Materials and methods

Cell lines

SKOV3 (Cat #HTB-77; ATCC) and L929 cells (Cat #CCL-1, RRID: CVCL_0462; ATCC) were obtained from the ATCC. HL-60 and Jurkat cells were obtained from the Denise Montell Lab at the University of California, Santa Barbara. HCT116 cells were obtained from the Chris Richardson Lab at the University of California, Santa Barbara. PANC-1 cells were obtained from the Angela Pitenis Lab at the University of California, Santa Barbara. Lenti-X 293T cells were purchased from Takara (Cat #632180). SKOV3 and HCT116 cells were cultured in McCoy's 5A (16-600-108; Thermo Fisher Scientific), 10% FBS, and 1% PSG. PANC-1, L929, and 293T cells were cultured in DMEM (11965118; Thermo Fisher Scientific), 10% FBS, and 1% PSG. HL-60 cells were cultured in IMDM (12440061; Thermo Fisher Scientific). Raji and Jurkat cells were cultured in RPMI with 1% Glutimax (72400120; Thermo Fisher Scientific), 10% FBS, and 1% PSG. Cells were routinely tested for mycoplasma. Cells were used for <20 passages.

Lentivirus production

pMD2.G (gift from Didier Trono, École Polytechnique Federal de Lausanne (EPFL), Lausanne, Switzerland, VSV-G plasmid, plasmid 12259; Addgene), pCMV-dR8.2 (gift from Bob Weinberg, MIT, Cambridge, MA, USA, plasmid 8455; Addgene) (Stewart et al., 2003), and our target construct were cloned into the pHR backbone. Transgene plasmids were transfected with lipofectamine LTX (15338-100; Invitrogen) into HEK293T cells to generate lentivirus. The media was harvested at 72 h, drawn through a 0.45-µm filter, and concentrated in LentiX (631232; Takara Biosciences).

Bone marrow–derived macrophage production and culture

Male and female C57BL/6 mice (RRID:IMSR_JAX:000664) between the ages of 6–10 wk were sacrificed by CO_2 inhalation. Hips, femurs, tibia, and shoulders were dissected, and bone marrow was isolated according to Weischenfelt and Porse (Weischenfeldt and Porse, 2008). Bone marrow cells were differentiated in complete RPMI supplemented with 20% L929-conditioned media for 7 days in a humidified incubator with 5% CO_2 at 37°C. Fresh BMDM media was applied every 2–3 days. Macrophage progenitors were infected with the lentiviruses Her2 CAR, GFP-CAAX, or mCh-CAAX on day 5 after harvest. For each experiment, the harvested bone marrow cells were pooled and randomly allocated to the experimental conditions prior to lentiviral infection. Differentiated BMDMs were used for experiments from 7 to 10 days. Macrophages were included in the study if differentiation >80% stained double positive for CD11b and F4/80 staining. There was no attrition in this study.

Mice were housed in the UCSB Animal Resource Center, an AAALAC-accredited animal facility. Procedures were performed in accordance with Institutional Animal Care and Use Committee guidelines and approved protocol (#975).

Spheroid production

Low-adhesion dishes were prepared by coating the wells of a tissue culture–treated 96-well plate (087722C; Thermo Fisher Scientific) with 1.5% agarose. SKOV3 cells were plated at 8,000 cells per well in normal growth medium supplemented with 2.5% of reconstituted basement membrane (rBM), Matrigel (CB-40230C; Corning). Plates were centrifuged at 1,000 rpm for 10 min at 4°C to aggregate a plane of cells for spheroid formation. Cells were incubated for 72 h at 37°C, upon which compact spheroids could be observed.

Plasmids

Her2 CAR GFP was constructed in the pHR vector as follows: Signal peptide (MQSGTHWRVLGLCLLSVGVWGQD) derived from CD3ε, extracellular anti-HER2 (4D5-8) scFv (Carter et al., 1992), stalk and TM aa 138–206 CD8 (UniProt Q96QR6_HUMAN), R (single arginine insertion from cloning process), cytoplasmic domain (aa 45–86) of the Fc γ-chain UniProtKB P20491 (FCERG_MOUSE), linker GSGS, and fluorophore: mGFP.

H2B-iRFP contains H2B (UniProt H2B1B_HUMAN) inserted into the pHR vector; fluorophore $iRFP_{710}$.

CDH1-eGFP contains CDH1 (133805; AddGene [Toda et al., 2018]) inserted into the puromycin-resistant and doxycycline-inducible pCW57 vector (71782; AddGene [Barger et al., 2019]); fluorophore eGFP.

The GFP-CAAX in the pHR vector (Morrissey et al., 2018) contains eGFP fused to a C-terminal CAAX targeting motif: KMSKDGKKKKKKSKTKCVIM.

mCh-CAAX in the pHR vector (Morrissey et al., 2018) contains mCh fused to a C-terminal CAAX targeting motif: KMSKDGKKKKKKSKTKCVIM.

Downloaded from http://rupress.org/jcb/article-pdf/224/11/e202502034/1950889/jcb_202502034.pdf by guest on 12 May 2026

The iRFP-CAAX in the pHR vector (170464; AddGene [Harris et al., 2021]) contains an $iRFP_{670}$ fused to a C-terminal CAAX targeting motif: KMSKDGKKKKKKSKTKCVIM.

Flow cytometry measurement of trogocytosis and phagocytosis

For adherent solid tumor cell lines, 35,000 cells were plated in 1 well of a 12-well dish and incubated overnight prior to the experiment. For suspended targets, including solid or diffuse tumors, 75,000 cells were directly added to 1 well of a 12-well dish at the time of experimentation. These plating conditions both resulted in ∼75,000 cell targets at the time of the experiment. For antibody opsonization, purified mouse anti-human CD47 (323102, RRID:AB_756132; BioLegend) was spiked into the wells of cancer cells at a concentration of 5 µg/ml. To achieve a ∼1:1 ratio of effector to target cell ratio, 75,000 Her2 CAR or GFP BMDMs were added to each well. BMDMs and cancer cells were co-incubated for 2 h, harvested in 0.25% trypsin EDTA (25200072; Thermo Fisher Scientific), neutralized, and then washed in cold PBS. Samples were analyzed in an Attune NxT (Invitrogen). Further analysis was conducted in FlowJo. BMDMs were gated by GFP^+ single cells, then internalization of cancer cells was distinguished for trogocytosis by mCh^+/iRFP- and phagocytosis by $mCh^+/iRFP^+$ events.

In the initial characterization of Her2 CAR macrophage activity against $Her2^+$ SKOV3 (Fig. 1 B), GFP-CAAX, and Her2 CAR BMDMs were plated in 1 well of a 12-well dish. The following day, SKOV3 were trypsinized and dyed with CellTrace Far Red (C34572; Thermo Fisher Scientific) in suspension. The SKOV3 cells were then added to BMDMs at a 3:1 (target: effector) ratio for 3 h, and internalization was measured by flow cytometry.

Time-lapse microscopy of macrophage activity in 2D monolayers

Unless otherwise specified, SKOV3 and macrophage co-incubations were performed with adherent SKOV3 and macrophages added in suspension. 10,000 SKOV3 were plated in 1 well of a 96-well glass-bottom MatriPlate (MGB096-1-2-LG-L; Brooks) and incubated overnight to establish adhesion. SKOV3 count approximately doubled overnight, yielding 20,000 cells. To achieve a ∼1:1 effector to target cell ratio, 20,000 Her2 CAR or GFP BMDMs were added to each well the following day. Co-incubations were imaged using spinning disc microscopy (40 × 0.95 NA Plan Apo air) for 8–10 h with time intervals of 6 min or less. Internalized cancer cells were classified for trogocytosis or phagocytosis in ImageJ. Trogocytosis was classified as BMDMs that ingested fragments of the target cell membrane. Phagocytosis was classified as BMDMs that engulfed the target cell whole.

In Fig. 5 A and Fig. S4 A, suspended SKOV3 cells were added to adherent macrophages at the start of the time-lapse experiment at a 1:1 ratio of 20,000 macrophages:20,000 targets.

Mitotic mCh-CAAX SKOV3 were classified by the retraction of the membrane to a round mother cell, formation of a cleavage furrow, or the appearance of a daughter cell. Phagocytosis of a mitotic target was verified by any of the indicated hallmarks of mitosis.

Spheroid size measurements

After 72 h on low-adhesion plates, the resulting SKOV3 spheroids were transferred to a Matrigel dome of 50:50 rBM and NGM. BMDMs were added at 500,000 cells per dome to the liquid Matrigel. Domes were incubated at 37°C for 30 min to set the matrix before 500 µl of NGM was added to the well. Whole spheroids were removed from the incubator and imaged daily for 10 days via spinning disc microscopy (10 × 0.95 NA Plan Apo air). Large images were captured in Nikon Elements by stitching together a grid of four images using the large image tool (15% overlap). The diameter of the mCherry signal (mCherry-CAAX from SKOV3 cells and internalized mCherry in macrophages) was measured in both the X and Y dimensions in ImageJ. The X and Y diameters were averaged to obtain the final spheroid diameter.

Quantification of trogocytosis and phagocytosis in spheroids

Spheroid macrophage co-incubations were imaged via spinning disc microscopy (40× 1.15 NA WI). BMDM activity was characterized in ImageJ by using mCherry-CAAX and H2B-iRFP SKOV3 cells to distinguish trogocytosis ($mCherry^+$ and $iRFP^-$) and phagocytosis ($mCherry^+$ and $iRFP^+$). 100 µm Z-stacks were captured at 2 µm steps. Only BMDMs that made contact with the spheroid were included in the analysis.

Macrophage invasion in spheroids

Using Imaris 10.1, 10x spheroid Z-stacks were cropped to fit the spheroid dimensions, reducing excess background signal. The SKOV3 fluorescent membrane signal was thresholded to generate a reconstructed spheroid surface. The reconstructed surface was overlaid on each slice of the Z-stack for ease of visualizing macrophages that had invaded into the spheroid.

Her2 immunofluorescent staining

10,000 mCh-CAAX SKOV3 were added to 1 well of a 96-well glass-bottom MatriPlate (MGB096-1-2-LG-L; Brooks) and incubated overnight to establish adhesion. GFP-CAAX or Her2 CAR BMDMs were added at a 1:1 ratio. The co-incubation was terminated after 2 h by the addition of fixative. Cells were fixed in 4% paraformaldehyde in PBS for 10 min, washed three times in 0.1% PBSTX, and then blocked in a solution of 3% BSA, 1X TBS, 0.1% Triton X, and 0.1% Na azide for 10 min. Cells were treated overnight with the primary antibody Human Anti-ErbB2 antibody, clone 4D5-8 (MCA6092, RRID:AB_2941663; Bio-Rad) at 1 µg/ml (1:1,000) and 4°C. Cells were washed three times with 0.1% PBSTX, then treated for 1 h with the secondary antibody Mouse anti Human IgG (Fc) (CH2 Domain):Alexa Fluor 647 (MCA2477A647, RRID:AB_3100823; Bio-Rad) at ∼3.33 µg/ml (1:300) and 4°C. Cells were washed three times with 0.1% PBSTX, treated with DAPI for 10 min, and then washed three times in PBS. Cells were imaged in PBS. Images were captured using the 100 × 1.49 NA oil immersion objective.

Antigen shaving experiments

35,000 mCh-CAAX H2B-iRFP SKOV3 were plated in 1 well of a 12-well dish and incubated overnight prior to the experiment. 75,000 Her2 CAR or GFP BMDMs were added to each well except

Downloaded from http://rupress.org/jcb/article-pdf/224/11/e202502034/1950889/jcb_202502034.pdf by guest on 12 May 2026

single-cell controls. BMDMs and cancer cells were co-incubated for 2 h, harvested in 0.25% trypsin EDTA, neutralized, and then blocked in incubation buffer (PBS +0.5% BSA) for 10 min. Cells were resuspended in incubation buffer for 30 min with the following antibodies run on independent samples: Brilliant Violet 421 isotype control (400157; RRID:AB_10897939; BioLegend), Anti-CD340 BV421 (324420; RRID:AB_2563990; BioLegend), Pacific blue anti-human HLA-A,B,C Antibody (311417; RRID:AB_493668; BioLegend), Pacific Blue Mouse IgG2a, κ Isotype Ctrl Antibody (400235; RRID:AB_493447; BioLegend), BV605 anti-human cd47, mouse IgG1 k, clone CC2C6 (323119; RRID:AB_2721546; BioLegend), and BV605 Mouse IgG1, κ Isotype Ctrl Antibody(400161; RRID:AB_11125373; BioLegend). Samples were triple washed in PBS and then analyzed in an Attune NxT. Further analysis was conducted in FlowJo to isolate the cancer cells and assess the median fluorescence intensity of each sample.

RGD peptide treatment

For RGD peptide–treated cells, 20,000 SKOV3 cells were seeded in media supplemented with 50 µg/ml of cilengitide trifluoroacetate salt (88968-51-6; VWR International). Media was aspirated and replaced with fresh media immediately before adding 20,000 macrophages. Experiments were conducted with GFP-CAAX BMDM in the presence or absence of antibody opsonization and with Her2 CAR BMDM or GFP-CAAX BMDM. For antibody opsonization, purified mouse anti-human CD47 (323102, RRID:AB_756132; BioLegend) was spiked into the wells of cancer cells at a concentration of 5 µg/ml. Trogocytosis and phagocytosis were measured by time-lapse microscopy as described above.

Focal adhesion CRISPR knockout generation and validation

Focal adhesion knockouts were generated by digesting the guide scaffold of LentiCRISPR v2 (plasmid 52961; Addgene) and replacing it with the top guides of ITGB1, ITGB5, ITGAV, and a nontargeting (NT) guide from the GeCKO v2 library (Table S1 [Sanjana et al., 2014]). mCh-CAAX H2B-iRFP SKOV3 were infected with the lentivirus, and infected cells were selected with puromycin.

Integrin knockouts were validated for absence of surface expression via antibody staining. The SKOV3 integrin knockout cell lines were harvested in 0.25% trypsin EDTA, neutralized, washed in cold PBS, and then blocked in incubation buffer for 10 min. Cells were resuspended in incubation buffer for 30 min with the following antibodies: FITC ITGB5 IgG1 kappa (11-0497-41, RRID:AB_2043843; Thermo Fisher Scientific), FITC isotype control IgG1 kappa (11-4714-81, RRID:AB_470021; Thermo Fisher Scientific), FITC ITAV/CD51 IgG2a kappa (327907, RRID:AB_940558; BioLegend), or FITC isotype control IgG2a kappa (400210, RRID:AB_326458; BioLegend). Samples were triple washed in PBS and then analyzed in an Attune NxT. Analysis was conducted in FlowJo to assess the median fluorescence intensity of each sample.

Focal adhesion staining

10,000 SKOV3 with NT, ITGB1, ITGB5, or ITGAV CRISPR guides (Table S1) were added to 1 well of a 96-well glass-bottom MatriPlate (MGB096-1-2-LG-L; Brooks) and incubated overnight to establish adhesion. Cells were fixed in 4% paraformaldehyde in PBS for 10 min, washed three times in 0.1% PBSTX, and then blocked in a solution of 3% BSA, 1X TBS, 0.1% Triton X, and 0.1% Na Azide for 10 min. Cells were treated overnight at 4°C with the primary antibody Paxillin (E6R6Z) Rabbit mAb (50195T, RRID: AB_3698765; Cell Signaling) at 1 µg/ml (1:1,000). Cells were washed three times with 0.1% PBSTX, then treated for 1 h with the secondary antibody Anti-rabbit IgG (H+L), F(ab′)2 Fragment; Alexa Fluor 647 Conjugate (4414, RRID:AB_10693544; Cell Signaling) at ∼3.33 µg/ml (1:300) and 4°C. Cells were also treated with Acti-stain 488 phalloidin at this step (PHDG1-A; Cytoskeleton) at 100 nM. Cells were washed three times with 0.1% PBSTX, treated with DAPI for 10 min, and then washed three times in PBS. Cells were imaged in PBS. Images were captured using the 100 × 1.49 NA oil immersion objective. Focal adhesions were quantified in ImageJ following the method outlined by Horzum, Ozdil, and Pesen-Okvur (Horzum et al., 2014).

E-cadherin overexpression

iRFP$_{670}$-CAAX or H2B-iRFP$_{710}$ Raji were infected with CDH1-eGFP and underwent puromycin selection to select for infected cells. 20,000 cells were plated into 1 well of a 12 well. To achieve the E-cadherin overexpression, cells were treated with doxycycline for 72 h prior to the experiment. At the time of the experiment, control iRFP$_{670}$-CAAX or H2B-iRFP$_{710}$ Raji was added at 450,000 cells to 1 well of a 12 well, adjusted to the count of the E-cadherin overexpression cells. Cells were treated with purified mouse anti-human CD47 (323102, RRID:AB_756132; BioLegend) at a concentration of 5 µg/ml. 450,000 BMDMs were seeded into each well and co-incubated for 2 h. BMDMs, and cancer cells were co-incubated for 2 h, harvested in 0.25% trypsin EDTA, neutralized, and then washed in cold PBS. Samples were analyzed in an Attune NxT. Further analysis was conducted in FlowJo. BMDMs were gated by area/aspect ratio, mCh$^+$ events. Within the mCh$^+$ BMDM gate, phagocytosis was determined by the iRFP$^+$ events from H2B-iRFP$_{710}$ samples, whereas total activity was determined by the iRFP$^+$ events from iRFP$_{670}$-CAAX.

Cell cycle arrest

Cells were treated with 0.1 uM paclitaxel (P3456; Thermo Fisher Scientific) or 1uM STLC (164739-5G; Sigma-Aldrich) for 20 h prior to the experiment. To quantify cell cycle arrest, SKOV3 cells were infected with the FUCCI cell cycle reporter mCherry(G1)/BFP(S/G2) (plasmid 132429; Addgene) (Sato et al., 2019). mCherry$^+$ cells were considered to be in G1 and BFP$^+$ cells were counted as S/G2/M. SKOV3 were co-incubated with either GFP-CAAX or Her2 CAR BMDMs. Time-lapse imaging was used to measure phagocytosis as described above. Imaging was restricted to 4 h as a precaution to avoid a decrease in the viability of cells that have been locked in mitosis for >24 h.

Phosphatidylserine staining

To measure phosphatidylserine, cells were stained with Pacific Blue Annexin (640918, RRID:AB_1279046; BioLegend). 35,000 SKOV3 cells were plated into 1 well of a 12 well and incubated

Downloaded from http://rupress.org/jcb/article-pdf/224/11/e202502034/1950889/jcb_202502034.pdf by guest on 12 May 2026

overnight before treatment with a mitotic inhibitor for 20 h. SKOV3 treated with 250 µM hydrogen peroxide for 20 h served as a positive control for death. Cells were harvested in 0.25% trypsin EDTA, neutralized, washed in cold PBS, and then blocked in incubation buffer for 10 min. Cells were resuspended in annexin binding buffer for 30 min with Pacific Blue Annexin. Samples were triple washed in PBS and then analyzed in an Attune NxT.

Phagocytosis of apoptotic corpses

Apoptosis was induced via staurosporine according to Wu et al. (2024). 2 million Jurkats were added to 1 well of a 6 well. Staurosporine was added to the NGM at a concentration of 0.5 µg/ml. Cells were incubated at 37°C for 16 h. An aliquot of the untreated and treated cells was used to measure the level of phosphatidylserine exposure. This was achieved by washing the cells in cold PBS, blocking in incubation buffer for 10 min, and resuspending in annexin binding buffer for 30 min with Pacific Blue Annexin. Samples were triple washed in PBS and then analyzed in an Attune NxT. Additionally, the working stocks of the untreated and treated cells were stained with Hoechst for 10 min. Cells were washed three times in RPMI to remove free Hoechst. Jurkats and GFP-CAAX or Her2 CAR BMDM were each seeded at 100,000 cells per 1 well of a 12-well dish. Cells were co-incubated for 2 h at 37°C, harvested via cold PBS EDTA, and then resuspended in PBS, then analyzed in an Attune NxT.

Detection of apoptosis via caspase

mCh-CAAX SKOV3 were infected with lentivirus encoding a caspase activity sensor, GC3AI (gift from Binghui Li, Tianjin Medical University Cancer Institute and Hospital, Tianjin, China, plasmid #78910; Addgene) (Zhang et al., 2013), and infected cells were selected with puromycin. 20,000 mCh-CAAX GC3AI SKOV3 were added to 1 well of a 96-well glass-bottom MatriPlate and incubated overnight to establish adhesion. GFP-CAAX or Her2 CAR BMDMs were added at a ratio of 1:1. Co-incubations were imaged under live cell time-lapse for 12 h during the 24- to 36-h window after seeding the macrophages. The GC3AI sensor is cleaved by caspases, causing the nonfluorescent indicator to fluoresce in the GFP channel. Caspase sensor activation was quantified as ratio of number of SKOV3 cells with caspase reporter activity versus total number of SKOV3 cells.

Microscopy

All fluorescent images were acquired on a spinning disc confocal microscope (Nikon Ti2-E inverted microscope with a Yokogawa CSU-W1 spinning disk unit and a Hamamatsu Orca Fusion BT scMos camera). Objectives included 10× 0.45 NA Plan Apo air, 40 × 0.95 NA Plan Apo air, 40 × 1.15 NA water immersion, and a 100 × 1.49 NA oil immersion. The microscope is equipped with a piezo Z drive. Temperature (37°C), CO_2 (5%), and humidity were controlled via an OkoLabs stage top incubator. Image acquisition was controlled using Nikon Elements. Live-cell imaging was done in standard RPMI cell media. The specific fluorochromes are indicated in each figure legend. 2D images were viewed and analyzed in ImageJ. 3D spheroids were visualized in Imaris.

Bright-field images were acquired on an inverted ECHO Revolve with the 10 × 0.35 NA Plan Apo air objective. Image acquisition was controlled using ECHO software.

Statistical analysis

All statistical analyses were performed in Prism 10 (GraphPad) and presented as mean values and SEM. Figure legends indicate the statistical test performed and the number of biological replicates. For the majority of our studies, we performed four biological replicates. This was based on a power analysis using preliminary data at the start of this study. In flow cytometry experiments, three technical replicates were averaged to calculate the biological replicate. Where possible, we used automated quantification pipelines or blinded the analyzer to remove bias.

Online supplemental material

Fig. S1, related to Fig. 1, shows that apoptotic corpses are phagocytosed equivalently in control GFP and Her2 CAR BMDMs. Fig. S2; related to Fig. 2 shows macrophage phagocytosis and trogocytosis in 3D Spheroids. Fig. S3, related to Fig. 3, shows that Her2 CAR macrophages cause caspase activation in some SKOV3 cells, and Her2 antigen is stripped from apparently viable cells. Fig. S4, related to Fig. 5, shows that adhesion of SKOV3 limits phagocytosis and validation of integrin knockouts. Fig. S5, related to Fig. 7, shows that STLC and paclitaxel do not cause widespread phosphatidylserine exposure after 24 h, and mitotic inhibitors increased the population of Raji cells in S/G2/M. Video 1 shows an Her2 CAR macrophage phagocytosing an SKOV3 cell, related to Fig. 1 C. Video 2 shows an Her2 CAR macrophage trogocytosing an SKOV3 cell, related to Fig. 1 C. Video 3 shows that Her2 CAR macrophages infiltrate an SKOV3 spheroid. Video 4 shows that GFP-CAAX macrophages infiltrate an SKOV3 spheroid. Video 5 shows an Her2 CAR macrophage phagocytosing an SKOV3 cell in 3D spheroid. Video 6 shows an Her2 CAR macrophage phagocytosing a dividing SKOV3 cell, related to Fig. 7 A. Table S1 shows sgRNA focal adhesion components. Data S1 shows Source data for Fig. 2 B.

Data availability

The data underlying Fig. 2 are available in the online supplemental material. All other data are available from the corresponding author upon reasonable request.

Acknowledgments

We thank the members of the Morrissey Lab for their constructive feedback and advice. We also thank Ryan Stowers for advice on the 3D culture system.

This work was supported by NIGMS R35 GM146935 and the University of California Cancer Research Coordinating Committee seed grant C23CR5592. Meghan A. Morrissey is a Nadia's Gift Foundation Innovator of the Damon Runyon Cancer Research Foundation (DRR-85-25). Kirstin R. Rollins was supported by the UCSB Graduate Division Graduate Research Mentorship Program Fellowship and UCSB Graduate Division Research Accelerator Award. We acknowledge the use of the NRI-MCDB Microscopy Facility (Imaris) supported by the NIH:

Downloaded from http://rupress.org/jcb/article-pdf/224/11/e202502034/1950889/jcb_202502034.pdf by guest on 12 May 2026

1S10 ODO010610-01A1. We acknowledge the use of the Biological Nanostructures Laboratory within the California NanoSystems Institute, supported by the University of California, Santa Barbara, and the University of California, Office of the President. Illustrations were prepared in BioRender. Meghan A. Morrissey reports a patent US No 11,041,023 licensed to "Myeloid Therapeutics" and a patent PCT/US2022/078774 licensed to "Inceptor Bio."

Author contributions: Kirstin R. Rollins: conceptualization, formal analysis, funding acquisition, investigation, methodology, project administration, validation, visualization, and writing—original draft, review, and editing. Sareen Fiaz: conceptualization, formal analysis, investigation, and methodology. Ishwaree Datta: formal analysis, investigation, and methodology. Meghan A. Morrissey: conceptualization, funding acquisition, project administration, supervision, and writing—original draft, review, and editing.

Disclosures: All authors have completed and submitted the ICMJE Form for Disclosure of Potential Conflicts of Interest. M.A. Morrissey reported a patent to US No 11,041,023 licensed "Myeloid Therapeutics" and a patent to PCT/US2022/078774 licensed "Inceptor Bio." No other disclosures were reported.

Submitted: 6 February 2025
Revised: 10 July 2025
Accepted: 27 August 2025

References

Abdu, Y., C. Maniscalco, J.M. Heddleston, T.-L. Chew, and J. Nance. 2016. Developmentally programmed germ cell remodelling by endodermal cell cannibalism. *Nat. Cell Biol.* 18:1302–1310. https://doi.org/10.1038/ncb3439

Akhmanova, M., S. Emtenani, D. Krueger, A. Gyoergy, M. Guarda, M. Vlasov, F. Vlasov, A. Akopian, A. Ratheesh, De S. Renzis, and D.E. Siekhaus. 2022. Cell division in tissues enables macrophage infiltration. *Science*. 376:394–396. https://doi.org/10.1126/science.abj0425

Arandjelovic, S., and K.S. Ravichandran. 2015. Phagocytosis of apoptotic cells in homeostasis. *Nat. Immunol.* 16:907–917. https://doi.org/10.1038/ni.3253

Barger, C.J., C. Branick, L. Chee, and A.R. Karpf. 2019. Pan-cancer analyses reveal genomic features of FOXM1 overexpression in cancer. *Cancers*. 11: 251. https://doi.org/10.3390/cancers11020251

Beningo, K.A., and Y.-L. Wang. 2002. Fc-receptor-mediated phagocytosis is regulated by mechanical properties of the target. *J. Cell Sci.* 115:849–856. https://doi.org/10.1242/jcs.115.4.849

Bettadapur, A., H.W. Miller, and K.S. Ralston. 2020. Biting off what can be chewed: Trogocytosis in health, infection, and disease. *Infect. Immun.* 88:e00930-19, https://doi.org/10.1128/IAI.00930-19

Beum, P.V., E.M. Peek, M.A. Lindorfer, F.J. Beurskens, P.J. Engelberts, P.W.H.I. Parren, J.G.J. van de Winkel, and R.P. Taylor. 2011. Loss of CD20 and bound CD20 antibody from opsonized B cells occurs more rapidly because of trogocytosis mediated by Fc receptor-expressing effector cells than direct internalization by the B cells. *J. Immunol.* 187: 3438–3447. https://doi.org/10.4049/JIMMUNOL.1101189

Brancolini, C., D. Lazarevic, J. Rodriguez, and C. Schneider. 1997. Dismantling cell–cell contacts during apoptosis is coupled to a caspase-dependent proteolytic cleavage of β-Catenin. *J. Cell Biol.* 139:759–771. https://doi.org/10.1083/jcb.139.3.759

Carter, P., L. Presta, C.M. Gorman, J.B. Ridgway, D. Henner, W.L. Wong, A.M. Rowland, C. Kotts, M.E. Carver, and H.M. Shepard. 1992. Humanization of an anti-p185HER2 antibody for human cancer therapy. *Proc. Natl. Acad. Sci. USA*. 89:4285–4289. https://doi.org/10.1073/pnas.89.10.4285

Casey, R.C., K.M. Burleson, K.M. Skubitz, S.E. Pambuccian, T.R. Oegema, L.E. Ruff, and A.P. Skubitz. 2001. Beta 1-integrins regulate the formation and adhesion of ovarian carcinoma multicellular spheroids. *Am. J. Pathol.* 159:2071–2080. https://doi.org/10.1016/s0002-9440(10)63058-1

Chao, M.P., A.A. Alizadeh, C. Tang, J.H. Myklebust, B. Varghese, S. Gill, M. Jan, A.C. Cha, C.K. Chan, B.T. Tan, et al. 2010. Anti-CD47 antibody synergizes with rituximab to promote phagocytosis and eradicate non-hodgkin lymphoma. *Cell*. 142:699–713. https://doi.org/10.1016/j.cell.2010.07.044

Chen, X., X. Song, K. Li, and T. Zhang. 2019. FcγR-Binding is an important functional attribute for immune checkpoint antibodies in cancer immunotherapy. *Front. Immunol.* 10:292. https://doi.org/10.3389/fimmu.2019.00292

Cornell, C.E., A. Chorlay, D. Krishnamurthy, N.R. Martin, L. Baldauf, and D.A. Fletcher. 2024. Target cell tension regulates macrophage trogocytosis. *bioRxiv*. https://doi.org/10.1101/2024.12.02.626490 (Preprint posted December 05, 2024).

Cruet-Hennequart, S., S. Maubant, J. Luis, P. Gauduchon, C. Staedel, and S. Dedhar. 2003. Alpha(v) integrins regulate cell proliferation through integrin-linked kinase (ILK) in ovarian cancer cells. *Oncogene*. 22: 1688–1702. https://doi.org/10.1038/sj.onc.1206347

Dahan, R., B.C.Barnhart, F.Li, A.P.Yamniuk, A.J.Korman, and J.V.Ravetch. 2016. Therapeutic activity of agonistic, human Anti-CD40 monoclonal antibodies requires selective FcγR engagement. *Cancer Cell*. 29:820–831. https://doi.org/10.1016/j.ccell.2016.05.001

Davidson, B., I. Goldberg, R. Reich, L. Tell, H.P. Dong, C.G. Trope', B. Risberg, and J. Kopolovic. 2003. AlphaV- and beta1-integrin subunits are commonly expressed in malignant effusions from ovarian carcinoma patients. *Gynecol. Oncol.* 90:248–257. https://doi.org/10.1016/s0090-8258(03)00321-4

de Visser, K.E., and J.A. Joyce. 2023. The evolving tumor microenvironment: From cancer initiation to metastatic outgrowth. *Cancer Cell*. 41:374–403. https://doi.org/10.1016/j.ccell.2023.02.016

Dechantsreiter, M.A., E. Planker, B. Mathä, E. Lohof, G. Hölzemann, A. Jonczyk, S.L. Goodman, and H. Kessler. 1999. N-Methylated cyclic RGD peptides as highly active and selective alpha(V)beta(3) integrin antagonists. *J. Med. Chem.* 42:3033–3040. https://doi.org/10.1021/jm970832g

Desgrosellier, J.S., and D.A. Cheresh. 2010. Integrins in cancer: Biological implications and therapeutic opportunities. *Nat. Rev. Cancer*. 10:9–22. https://doi.org/10.1038/nrc2748

Dix, C.L., H.K. Matthews, M. Uroz, S. McLaren, L. Wolf, N. Heatley, Z. Win, P. Almada, R. Henriques, M. Boutros, et al. 2018. The role of mitotic cell-substrate adhesion Re-modeling in animal cell division. *Dev. Cell*. 45: 132–145.e3. https://doi.org/10.1016/j.devcel.2018.03.009

Dooling, L.J., J.C. Andrechak, B.H. Hayes, S. Kadu, W. Zhang, R. Pan, M. Vashisth, J. Irianto, C.M. Alvey, L. Ma, and D.E. Discher. 2023. Cooperative phagocytosis of solid tumours by macrophages triggers durable anti-tumour responses. *Nat. Biomed. Eng.* 7:1081–1096. https://doi.org/10.1038/s41551-023-01031-3

Dooling, L.J., A.A. Anlaş, M.P. Tobin, N.M. Ontko, T. Marchena, M. Wang, J.C. Andrechak, and D.E. Discher. 2024. Clustered macrophages cooperate to eliminate tumors via coordinated intrudopodia. *bioRxiv*. https://doi.org/10.1101/2024.09.19.613918 (Preprint posted September 20, 2024).

Fesnak, A.D., C.H. June, and B.L. Levine. 2016. Engineered T cells: The promise and challenges of cancer immunotherapy. *Nat. Rev. Cancer*. 16: 566–581. https://doi.org/10.1038/nrc.2016.97

Finotti, G., E. Pietronigro, C. Balanzin, S. Lonardi, G. Constantin, M.P. Chao, C. Tecchio, W. Vermi, and M.A. Cassatella. 2023. Slan$^+$ monocytes kill cancer cells coated in therapeutic antibody by trogoptosis. *Cancer Immunol. Res.* 11: 1538–1552. https://doi.org/10.1158/2326-6066.CIR-23-0239

Freeman, S., and S. Grinstein. 2021. Promoters and antagonists of phagocytosis: A plastic and tunable response. *Annu. Rev. Cell Dev. Biol.* 37:89–114. https://doi.org/10.1146/annurev-cellbio-120219-055903

Gao, X., R.S. Carpenter, P.E. Boulais, D. Zhang, C.R. Marlein, H. Li, M. Smith, D.J. Chung, M. Maryanovich, B. Will, et al. 2024. Regulation of the hematopoietic stem cell pool by C-Kit-associated trogocytosis. *Science*. 385: eadp2065. https://doi.org/10.1126/science.adp2065

Giordano, S.H., M.A.B. Franzoi, S. Temin, C.K. Anders, S. Chandarlapaty, J.R. Crews, J.J. Kirshner, I.E. Krop, N.U. Lin, A. Morikawa, et al. 2022. Systemic therapy for advanced human epidermal growth factor receptor 2–Positive breast cancer: ASCO guideline update. *J. Clin. Oncol.* 40:2612–2635. https://doi.org/10.1200/JCO.22.00519

Gordon, S. 2016. Phagocytosis: An immunobiologic process. *Immunity*. 44: 463–475. https://doi.org/10.1016/j.immuni.2016.02.026

Greiner, D., Q. Xue, T.Q. Waddell, E. Kurudza, P. Chaudhary, R.L. Belote, G. Dotti, R.L. Judson-Torres, M.Q. Reeves, S.H. Cheshier, and M. Roh-Johnson. 2025. Human CSPG4-targeting CAR-Macrophages inhibit

Downloaded from http://rupress.org/jcb/article-pdf/224/11/e202502034/1950889/jcb_202502034.pdf by guest on 12 May 2026

melanoma growth. *Oncogene*. 44:1665–1677. https://doi.org/10.1038/s41388-025-03332-0

Guerriero, J.L. 2018. Macrophages: The road less traveled, changing anticancer therapy. *Trends Mol. Med.* 24:472–489. https://doi.org/10.1016/j.molmed.2018.03.006

Gül, N., L. Babes, K. Siegmund, R. Korthouwer, M. Bögels, R. Braster, G. Vidarsson, T.L.M. ten Hagen, P. Kubes, and M. van Egmond. 2014. Macrophages eliminate circulating tumor cells after monoclonal antibody therapy. *J. Clin. Invest.* 124:812–823. https://doi.org/10.1172/JCI66776

Hamieh, M., A. Dobrin, A. Cabriolu, S.J.C. van der Stegen, T. Giavridis, J. Mansilla-Soto, J. Eyquem, Z. Zhao, B.M. Whitlock, M.M. Miele, et al. 2019. CAR T cell trogocytosis and cooperative killing regulate tumour antigen escape. *Nature*. 568:112–116. https://doi.org/10.1038/s41586-019-1054-1

Harris, M.J., M. Fuyal, and J.R. James. 2021. Quantifying persistence in the T-cell signaling network using an optically controllable antigen receptor. *Mol. Syst. Biol.* 17:e10091. https://doi.org/10.15252/msb.202010091

Heredia-Soto, V., A. Redondo, A. Berjón, M. Miguel-Martín, E. Díaz, R. Crespo, A. Hernández, L. Yébenes, A. Gallego, J. Feliu, et al. 2018. High-throughput 3-dimensional culture of epithelial ovarian cancer cells as preclinical model of disease. *Oncotarget*. 9:21893–21903. https://doi.org/10.18632/oncotarget.25098

Horwitz, S.B. 1994. Taxol (paclitaxel): Mechanisms of action. *Ann. Oncol.* 5: S3–S6

Horzum, U., B. Ozdil, and D. Pesen-Okvur. 2014. Step-by-step quantitative analysis of focal adhesions. *MethodsX*. 1:56–59. https://doi.org/10.1016/j.mex.2014.06.004

Hudrisier, D., J. Riond, H. Mazarguil, J.E. Gairin, and E. Joly. 2001. Cutting edge: CTLs rapidly capture membrane fragments from target cells in a TCR signaling-dependent manner. *J. Immunol.* 166:3645–3649. https://doi.org/10.4049/jimmunol.166.6.3645

Hudziak, R.M., G.D. Lewis, M. Winget, B.M. Fendly, H.M. Shepard, and A. Ullrich. 1989. p185HER2 monoclonal antibody has antiproliferative effects in vitro and sensitizes human breast tumor cells to tumor necrosis factor. *Mol. Cell. Biol.* 9:1165–1172. https://doi.org/10.1128/mcb.9.3.1165-1172.1989

Ivascu, A., and M. Kubbies. 2007. Diversity of cell-mediated adhesions in breast cancer spheroids. *Int. J. Oncol.* 31:1403–1413

Jaiswal, S., C.H.M. Jamieson, W.W. Pang, C.Y. Park, M.P. Chao, R. Majeti, D. Traver, N. van Rooijen, and I.L. Weissman. 2009. CD47 is upregulated on circulating hematopoietic stem cells and leukemia cells to avoid phagocytosis. *Cell*. 138:271–285. https://doi.org/10.1016/j.cell.2009.05.046

Joffe, A.M., M.H. Bakalar, and D.A. Fletcher. 2020. Macrophage phagocytosis assay with reconstituted target particles. *Nat. Protoc.* 15:2230–2246. https://doi.org/10.1038/s41596-020-0330-8

Joly, E., and D. Hudrisier. 2003. What is trogocytosis and what is its purpose? *Nat. Immunol.* 4:815. https://doi.org/10.1038/ni0903-815

Kennedy, A.D., P.V. Beum, M.D. Solga, D.J. DiLillo, M.A. Lindorfer, C.E. Hess, J.J. Densmore, M.E. Williams, and R.P. Taylor. 2004. Rituximab infusion promotes rapid complement depletion and acute CD20 loss in chronic lymphocytic leukemia. *J. Immunol.* 172:3280–3288. https://doi.org/10.4049/jimmunol.172.5.3280

Kern, N., R. Dong, S.M. Douglas, R.D. Vale, and M.A. Morrissey. 2021. Tight nanoscale clustering of Fcγ receptors using DNA origami promotes phagocytosis. *Elife*. 10:e68311. https://doi.org/10.7554/eLife.68311

Klichinsky, M., M. Ruella, O. Shestova, X.M. Lu, A. Best, M. Zeeman, M. Schmierer, K. Gabrusiewicz, N.R. Anderson, N.E. Petty, et al. 2020. Human chimeric antigen receptor macrophages for cancer immunotherapy. *Nat. Biotechnol.* 38:947–953. https://doi.org/10.1038/s41587-020-0462-y

Kochenderfer, J.N., S.A. Feldman, Y. Zhao, H. Xu, M.A. Black, R.A. Morgan, W.H. Wilson, and S.A. Rosenberg. 2009. Construction and preclinical evaluation of an Anti-CD19 chimeric antigen receptor. *J. Immunother.* 32: 689–702. https://doi.org/10.1097/CJI.0b013e3181ac6138

Lindorfer, M.A., and R.P. Taylor. 2022. FcγR-Mediated trogocytosis 2.0: Revisiting history gives rise to a unifying hypothesis. *Antibodies*. 11:45. https://doi.org/10.3390/antib11030045

Lock, J.G., M.C. Jones, J.A. Askari, X. Gong, A. Oddone, H. Olofsson, S. Göransson, M. Lakadamyali, M.J. Humphries, and S. Strömblad. 2018. Reticular adhesions are a distinct class of cell-matrix adhesions that mediate attachment during mitosis. *Nat. Cell Biol.* 20:1290–1302. https://doi.org/10.1038/s41556-018-0220-2

Majeti, R., M.P. Chao, A.A. Alizadeh, W.W. Pang, S. Jaiswal, K.D. Gibbs Jr., N. van Rooijen, and I.L. Weissman. 2009. CD47 is an adverse prognostic factor and therapeutic antibody target on human acute myeloid leukemia stem cells. *Cell*. 138:286–299. https://doi.org/10.1016/j.cell.2009.05.045

Manches, O., G. Lui, L. Chaperot, R. Gressin, J.-P. Molens, M.-C. Jacob, J.-J. Sotto, D. Leroux, J.-C. Bensa, and J. Plumas. 2003. In vitro mechanisms of action of rituximab on primary Non-Hodgkin lymphomas. *Blood*. 101: 949–954. https://doi.org/10.1182/blood-2002-02-0469

Marchesi, S., F. Montani, G. Deflorian, R. D'Antuono, A. Cuomo, S. Bologna, C. Mazzoccoli, T. Bonaldi, P.P. Di Fiore, and F. Nicassio. 2014. DEPDC1B coordinates De-adhesion events and cell-cycle progression at mitosis. *Dev. Cell*. 31:420–433. https://doi.org/10.1016/j.devcel.2014.09.009

Matlung, H.L., L. Babes, X.W. Zhao, M. van Houdt, L.W. Treffers, D.J. van Rees, K. Franke, K. Schornagel, P. Verkuijlen, H. Janssen, et al. 2018. Neutrophils kill antibody-opsonized cancer cells by trogoptosis. *Cell Rep.* 23:3946–3959.e6. https://doi.org/10.1016/J.CELREP.2018.05.082

Mercer, F., S.H. Ng, T.M. Brown, G. Boatman, and P.J. Johnson. 2018. Neutrophils kill the parasite trichomonas vaginalis using trogocytosis. *PLoS Biol.* 16:e2003885. https://doi.org/10.1371/JOURNAL.PBIO.2003885

Mishra, A.K., M. Rodriguez, A.Y. Torres, M. Smith, A. Rodriguez, A. Bond, M.A. Morrissey, and D.J. Montell. 2023. Hyperactive rac stimulates cannibalism of living target cells and enhances CAR-M-mediated cancer cell killing. *Proc. Natl. Acad. Sci. USA*. 120:e2310221120. https://doi.org/10.1073/pnas.2310221120

Möller, J., T. Lühmann, M. Chabria, H. Hall, and V. Vogel. 2013. Macrophages lift off surface-bound bacteria using a filopodium-lamellipodium hook-and-shovel mechanism. *Sci. Rep.* 3:2884. https://doi.org/10.1038/srep02884

Morrissey, M.A., A.P. Williamson, A.M. Steinbach, E.W. Roberts, N. Kern, M.B. Headley, and R.D. Vale. 2018. Chimeric antigen receptors that trigger phagocytosis. *Elife*. 7:e36688. https://doi.org/10.7554/eLife.36688

Nimmerjahn, F., and J.V. Ravetch. 2008. Fcgamma receptors as regulators of immune responses. *Nat. Rev. Immunol.* 8:34–47. https://doi.org/10.1038/nri2206

Osorio, J.C., P. Smith, D.A. Knorr, and J.V. Ravetch. 2023. The antitumor activities of anti-CD47 antibodies require Fc-FcγR interactions. *Cancer Cell*. 41:2051–2065.e6. https://doi.org/10.1016/j.ccell.2023.10.007

Park, H.-R., S.-E. Kim, B. Keam, H. Chung, S.H. Seok, S. Kim, M. Kim, T.M. Kim, J. Doh, D.-W. Kim, and D.S. Heo. 2022. Blockade of CD47 enhances the antitumor effect of macrophages in renal cell carcinoma through trogocytosis. *Sci. Rep.* 12:12546. https://doi.org/10.1038/s41598-022-16766-3

Petricevic, B., J. Laengle, J. Singer, M. Sachet, J. Fazekas, G. Steger, R. Bartsch, E. Jensen-Jarolim, and M. Bergmann. 2013. Trastuzumab mediates antibody-dependent cell-mediated cytotoxicity and phagocytosis to the same extent in both adjuvant and metastatic HER2/neu breast cancer patients. *J. Transl. Med.* 11:307. https://doi.org/10.1186/1479-5876-11-307

Ralston, K.S., M.D. Solga, N.M. Mackey-Lawrence, A. Bhattacharya, A. Bhattacharya, and W.A. Petri Jr. 2014. Trogocytosis by Entamoeba histolytica contributes to cell killing and tissue invasion. *Nature*. 508: 526–530. https://doi.org/10.1038/nature13242

Reiss, K.A., M.G. Angelos, E.C. Dees, Y. Yuan, N.T. Ueno, P.R. Pohlmann, M.L. Johnson, J. Chao, O. Shestova, J.S. Serody, et al. 2025. CAR-macrophage therapy for HER2-overexpressing advanced solid tumors: A phase 1 trial. *Nat. Med.* 31:1171–1182. https://doi.org/10.1038/s41591-025-03495-z

Sakaue-Sawano, A., H. Kurokawa, T. Morimura, A. Hanyu, H. Hama, H. Osawa, S. Kashiwagi, K. Fukami, T. Miyata, H. Miyoshi, et al. 2008. Visualizing spatiotemporal dynamics of multicellular cell-cycle progression. *Cell*. 132:487–498. https://doi.org/10.1016/j.cell.2007.12.033

Sanjana, N.E., O. Shalem, and F. Zhang. 2014. Improved vectors and genome-wide libraries for CRISPR screening. *Nat. Methods*. 11:783–784. https://doi.org/10.1038/nmeth.3047

Sato, H., B. Wu, F. Delahaye, R.H. Singer, and J.M. Greally 2019. Retargeting of macroH2A following mitosis to cytogenetic-scale heterochromatic domains. *J. Cell Biol.* 218:1810–1823. https://doi.org/10.1083/jcb.201811109

Settle, A.H., B.Y. Winer, M.M. de Jesus, L. Seeman, Z. Wang, E. Chan, Y. Romin, Z. Li, M.M. Miele, R.C. Hendrickson, et al. 2024. B2 integrins impose a mechanical checkpoint on macrophage phagocytosis. *Nat. Commun.* 15:8182. https://doi.org/10.1038/s41467-024-52453-9

Shi, Y., X. Fan, H. Deng, R.J. Brezski, M. Rycyzyn, R.E. Jordan, W.R. Strohl, Q. Zou, N. Zhang, and Z. An. 2015. Trastuzumab triggers phagocytic killing of high HER2 cancer cells in vitro and in vivo by interaction with Fcγ receptors on macrophages. *J. Immunol.* 194:4379–4386. https://doi.org/10.4049/jimmunol.1402891

Downloaded from http://rupress.org/jcb/article-pdf/224/11/e202502034/1950889/jcb_202502034.pdf by guest on 12 May 2026

Skoufias, D.A., S. DeBonis, Y. Saoudi, L. Lebeau, I. Crevel, R. Cross, R.H. Wade, D. Hackney, and F. Kozielski. 2006. S-Trityl-L-cysteine is a reversible, tight binding inhibitor of the human kinesin Eg5 that specifically blocks mitotic progression. *J. Biol. Chem.* 281:17559–17569. https://doi.org/10.1074/jbc.M511735200

Sloas, C., S. Gill, and M. Klichinsky. 2021. Engineered CAR-macrophages as adoptive immunotherapies for solid tumors. *Front. Immunol.* 12:783305. https://doi.org/10.3389/fimmu.2021.783305

Stewart, S.A., D.M. Dykxhoorn, D. Palliser, H. Mizuno, E.Y. Yu, D.S. An, D.M. Sabatini, I.S.Y. Chen, W.C. Hahn, P.A. Sharp, et al. 2003. Lentivirus-delivered stable gene silencing by RNAi in primary cells. *RNA*. 9: 493–501. https://doi.org/10.1261/rna.2192803

Suzuki, E., T.R. Kataoka, M. Hirata, K. Kawaguchi, M. Nishie, H. Haga, and M. Toi. 2015. Trogocytosis-mediated expression of HER2 on immune cells may be associated with a pathological complete response to trastuzumab-based primary systemic therapy in HER2-overexpressing breast cancer patients. *BMC Cancer*. 15:39. https://doi.org/10.1186/s12885-015-1041-3

Swain, S.M., M. Shastry, and E. Hamilton. 2023. Targeting HER2-positive breast cancer: Advances and future directions. *Nat. Rev. Drug Discov.* 22:101–126. https://doi.org/10.1038/s41573-022-00579-0

Toda, S., L.R. Blauch, S.K.Y. Tang, L. Morsut, and W.A. Lim. 2018. Programming self-organizing multicellular structures with synthetic cell-cell signaling. *Science*. 361:156–162. https://doi.org/10.1126/science.aat0271

Tofani, L.B., J.P. Abriata, M.T. Luiz, J.M. Marchetti, and K. Swiech. 2020. Establishment and characterization of an in vitro 3D ovarian cancer model for drug screening assays. *Biotechnol. Prog.* 36:e3034. https://doi.org/10.1002/btpr.3034

Uchida, J., Y. Hamaguchi, J.A. Oliver, J.V. Ravetch, J.C. Poe, K.M. Haas, and T.F. Tedder. 2004. The innate mononuclear phagocyte network depletes B lymphocytes through Fc receptor-dependent mechanisms during anti-CD20 antibody immunotherapy. *J. Exp. Med.* 199:1659–1669. https://doi.org/10.1084/jem.20040119

van Rees, D.J., P. Bouti, B. Klein, P.J.H. Verkuijlen, M. van Houdt, K. Schornagel, A.T.J. Tool, D. Venet, C. Sotiriou, S. El-Abed, et al. 2022. Cancer cells resist antibody-mediated destruction by neutrophils through activation of the exocyst complex. *J. Immunother. Cancer* 10:e004820. https://doi.org/10.1136/jitc-2022-004820

Van Wagoner, C.M., F. Rivera-Escalera, N.C. Jaimes-Delgadillo, C.C. Chu, C.S. Zent, and M.R. Elliott. 2023. Antibody-mediated phagocytosis in cancer immunotherapy. *Immunol. Rev.* 319:128–141. https://doi.org/10.1111/imr.13265

Velmurugan, R., D.K. Challa, S. Ram, R.J. Ober, and E.S. Ward. 2016. Macrophage-mediated trogocytosis leads to death of antibody-opsonized tumor cells. *Mol. Cancer Ther.* 15:1879–1889. https://doi.org/10.1158/1535-7163.MCT-15-0335

Weinhard, L., G.di Bartolomei, G. Bolasco, P. Machado, N.L. Schieber, U. Neniskyte, M. Exiga, A. Vadisiute, A. Raggioli, A. Schertel, et al. 2018. Microglia remodel synapses by presynaptic trogocytosis and spine head filopodia induction. *Nat. Commun.* 9:1228. https://doi.org/10.1038/s41467-018-03566-5

Weischenfeldt, J., and B. Porse. 2008. Bone marrow-derived macrophages (BMM): Isolation and applications. *CSH Protoc.* 2008:pdb.prot5080. https://doi.org/10.1101/pdb.prot5080

Weiskopf, K., and I.L. Weissman. 2015. Macrophages are critical effectors of antibody therapies for cancer. *MAbs*, 7, 303–310. https://doi.org/10.1080/19420862.2015.1011450

Williams, M.E., J.J. Densmore, A.W. Pawluczkowycz, P.V. Beum, A.D. Kennedy, M.A. Lindorfer, S.H. Hamil, J.C. Eggleton, and R.P. Taylor. 2006. Thrice-weekly low-dose rituximab decreases CD20 loss via shaving and promotes enhanced targeting in chronic lymphocytic leukemia. *J. Immunol.* 177, 7435–7443. https://doi.org/10.4049/jimmunol.177.10.7435

Wu, X., Z. Wang, T. Shern, and H. Zhang. 2024. Efferocytosis assay to quantify the engulfment and acidification of apoptotic cells by macrophages using flow cytometry. *STAR Protoc.* 5:103215. https://doi.org/10.1016/j.xpro.2024.103215

Zent, C.S., R.P. Taylor, M.A. Lindorfer, P.V. Beum, B. LaPlant, W. Wu, T.G. Call, D.A.Bowen, M.J. Conte, L.A. Frederick, et al. 2014. Chemoimmunotherapy for relapsed/refractory and progressive 17p13-deleted chronic lymphocytic leukemia (CLL) combining pentostatin, alemtuzumab, and low-dose rituximab is effective and tolerable and limits loss of CD20 expression by circulating CLL cells. *Am. J. Hematol.* 89:757–765. https://doi.org/10.1002/ajh.23737

Zhang, J., X. Wang, W. Cui, W. Wang, H. Zhang, L. Liu, Z. Zhang, Z. Li, G. Ying, N. Zhang, and B. Li. 2013. Visualization of caspase-3-like activity in cells using a genetically encoded fluorescent biosensor activated by protein cleavage. *Nat. Commun.* 4:2157. https://doi.org/10.1038/ncomms3157

Downloaded from http://rupress.org/jcb/article-pdf/224/11/e202502034/1950889/jcb_202502034.pdf by guest on 12 May 2026

Supplemental material

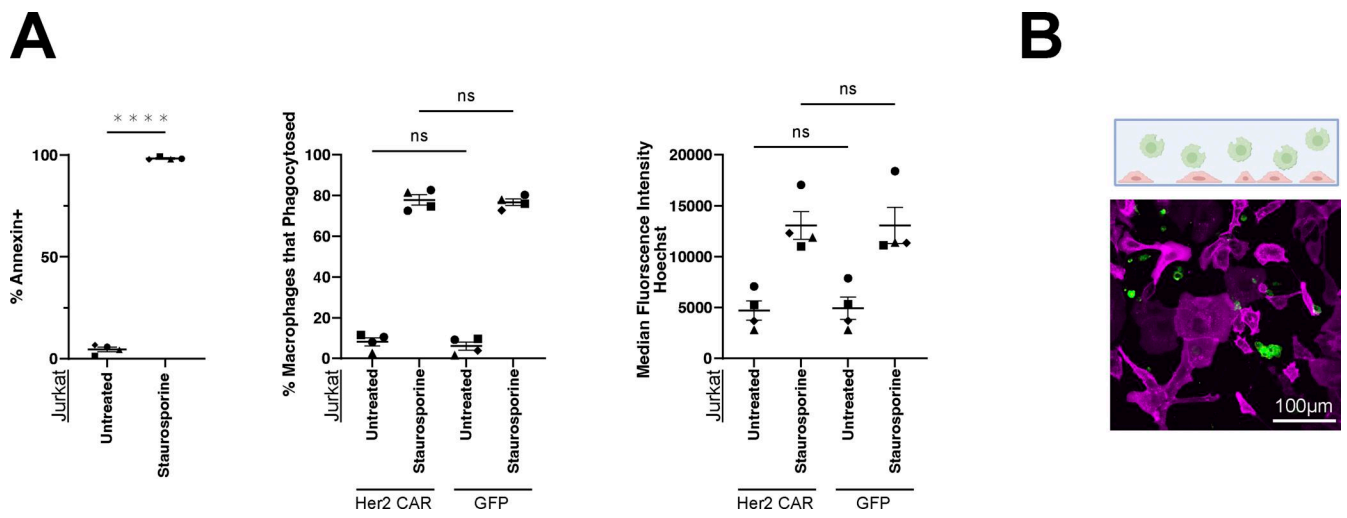

Figure S1. **Related to Fig. 1: Apoptotic corpses are phagocytosed equivalently in control GFP and Her2 CAR BMDMs. (A)** Apoptosis was induced in Jurkats by a 16 h treatment with 0.5 µg/ml Staurosporine. Jurkats were stained with annexin to confirm cell death. Jurkats were washed to remove staurosporine, stained with Hoechst, and then added to Her2 CAR and GFP control macrophages. The percent of macrophages internalizing an apoptotic corpse and the fluorescent intensity of internalized Hoechst were measured by flow cytometry. **(B)** A representative uncropped image shows the co-incubations presented in Fig. 1 C. Data in A were compared using one-way ANOVA with Holm–Sidak multiple comparison correction. *N* = 4 independent experiments. Bars represent the mean ± SEM. Data collected on the same day are annotated with the same shape point. **** denotes P < 0.00005. Scale bars in B denote 100 µm. BMDMs, bone marrow–derived macrophages.

Downloaded from http://rupress.org/jcb/article-pdf/224/11/e202502034/1950889/jcb_202502034.pdf by guest on 12 May 2026

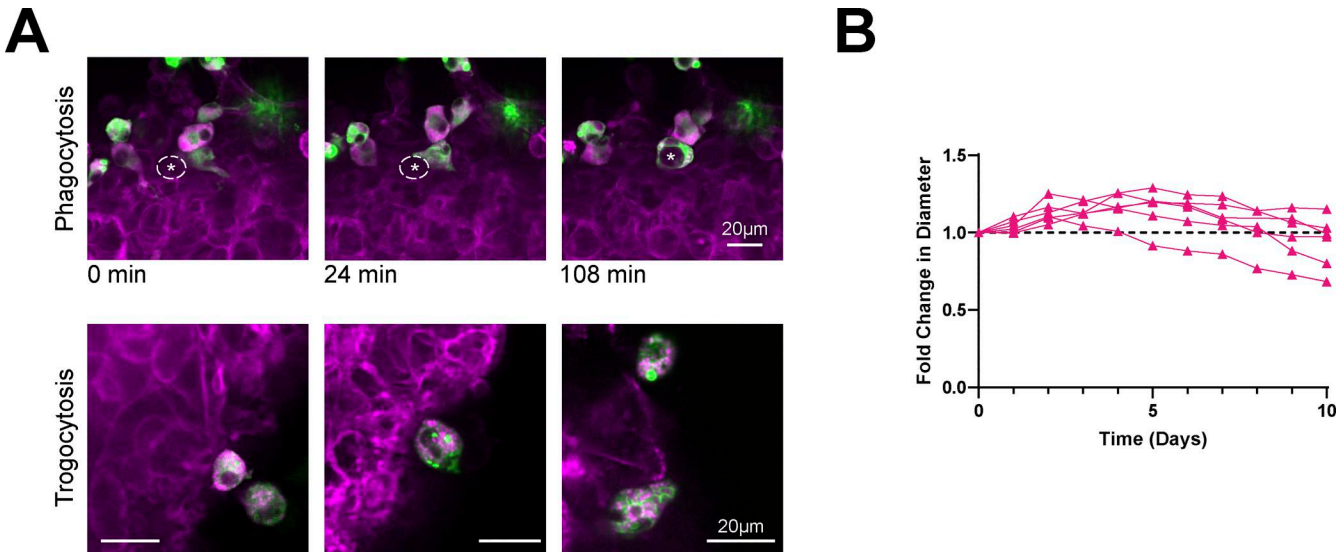

Figure S2. **Related to Fig. 2: Macrophage phagocytosis and trogocytosis in 3D spheroids. (A)** The top row shows an Her2 CAR GFP (green) macrophage phagocytosing an SKOV3 (mCherry-CAAX) cell in a 3D spheroid. The images are stills from Video 5. The dashed line and the asterisk denote the cell that will be phagocytosed. Scale bar is 20 μm. The bottom row shows still images of Her2 CAR GFP (green) macrophages that trogocytosed, as evidenced by the small bites of SKOV3 (mCherry-CAAX) cells within the macrophage. **(B)** Plot shows the fold change in diameter of each individual spheroids from the Her2 CAR treatment condition over the 10 days time course.

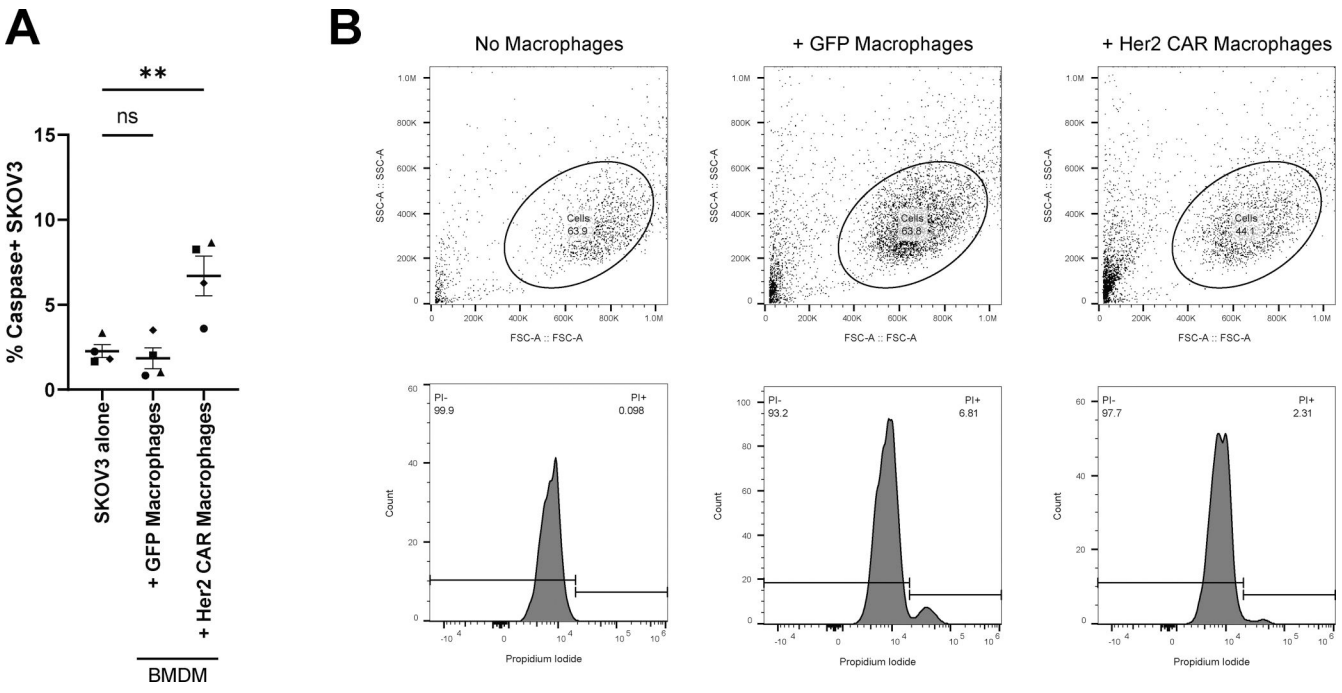

Figure S3. **Related to Fig. 3: Her2 CAR macrophages cause caspase activation in some SKOV3 cells, and Her2 antigen is stripped from apparently viable cells. (A)** SKOV3 cells were infected to express the caspase sensor GC3AI, which fluoresces when caspases are active. Her2 CAR or GFP control macrophages were added to the SKOV3 cells, and caspase activity was monitored beginning 24 h later. The graph depicts the percent of SKOV3 cells that activated caspases at any point during a 12-h time-lapse. **(B)** SKOV3 cells gated based on properties of FSC and SSC were confirmed to be primarily intact viable cells from the absence of propidium iodide. In A, data were compared using one-way ANOVA with Holm–Sidak multiple comparison correction. *N* = 4 independent experiments. Bars represent the mean ± SEM. Data collected on the same day are annotated with the same shape point. ** denotes P < 0.005.

Downloaded from http://rupress.org/jcb/article-pdf/224/11/e202502034/1950889/jcb_202502034.pdf by guest on 12 May 2026

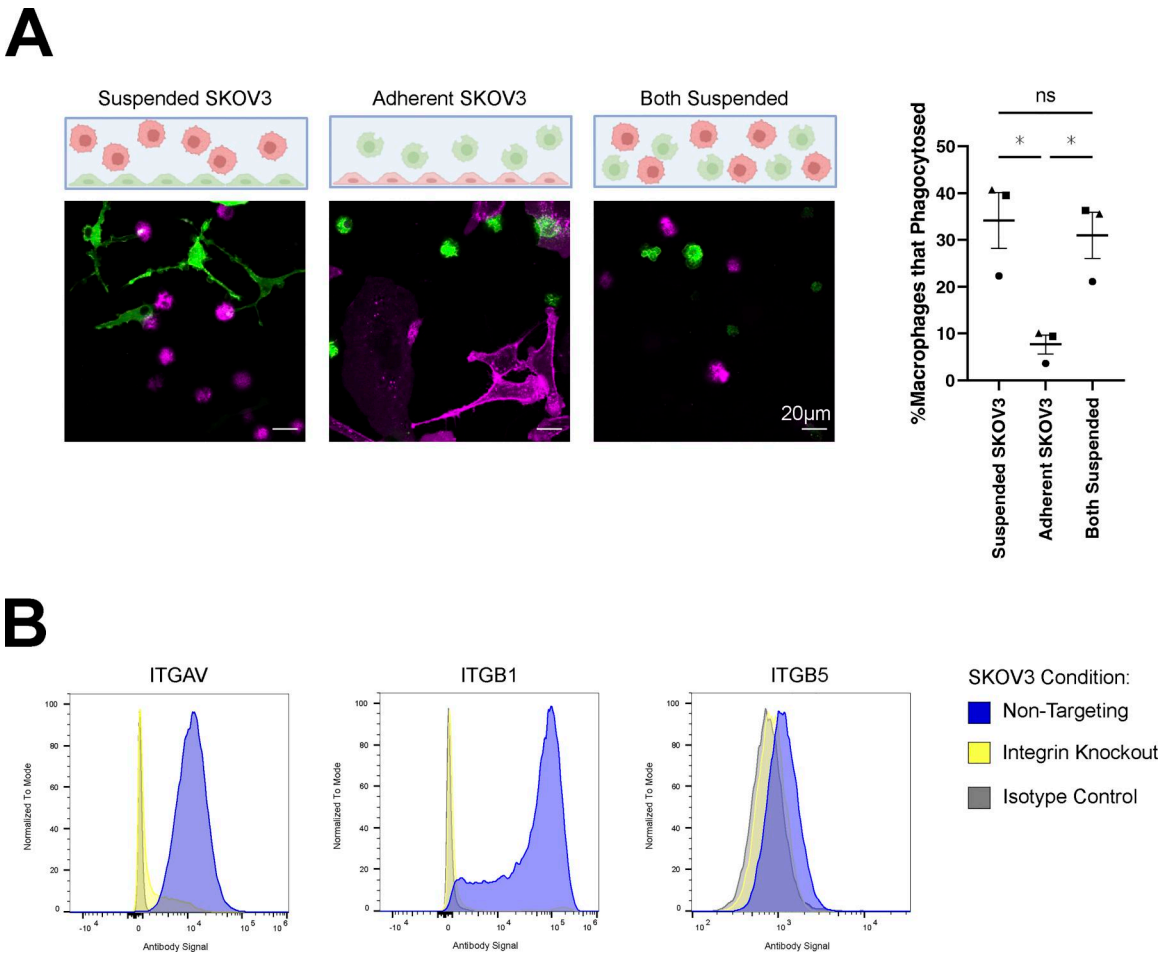

Figure S4. **Related to Fig. 5: Adhesion of SKOV3 limits phagocytosis and validation of integrin knockouts. (A)** SKOV3 cells (red) labeled with mCherry-CAAX were incubated with Her2 CAR GFP macrophages (green), and phagocytosis was measured during a 10-h time-lapse. The schematic shows the experimental setup with suspended SKOV3 cells and adherent macrophages, adherent SKOV3 cells and suspended macrophages, or both cells in suspension at the start of the time-lapse. Data were compared using one-way ANOVA with Holm–Sidak multiple comparison correction. $N = 3$ independent experiments. Bars represent the mean ± SEM. Data collected on the same day are annotated with the same shape point. * denotes $P < 0.05$. **(B)** SKOV3 cells were infected with a lentiviral construct encoding puromycin resistance, Cas9, and an sgRNA-targeting ITGAV, ITGB1, ITGB5, or a NT control. After puromycin selection, the polyclonal cell line was stained with an antibody targeting the relevant integrin subunit or an isotype control.

Downloaded from http://rupress.org/jcb/article-pdf/224/11/e202502034/1950889/jcb_202502034.pdf by guest on 12 May 2026

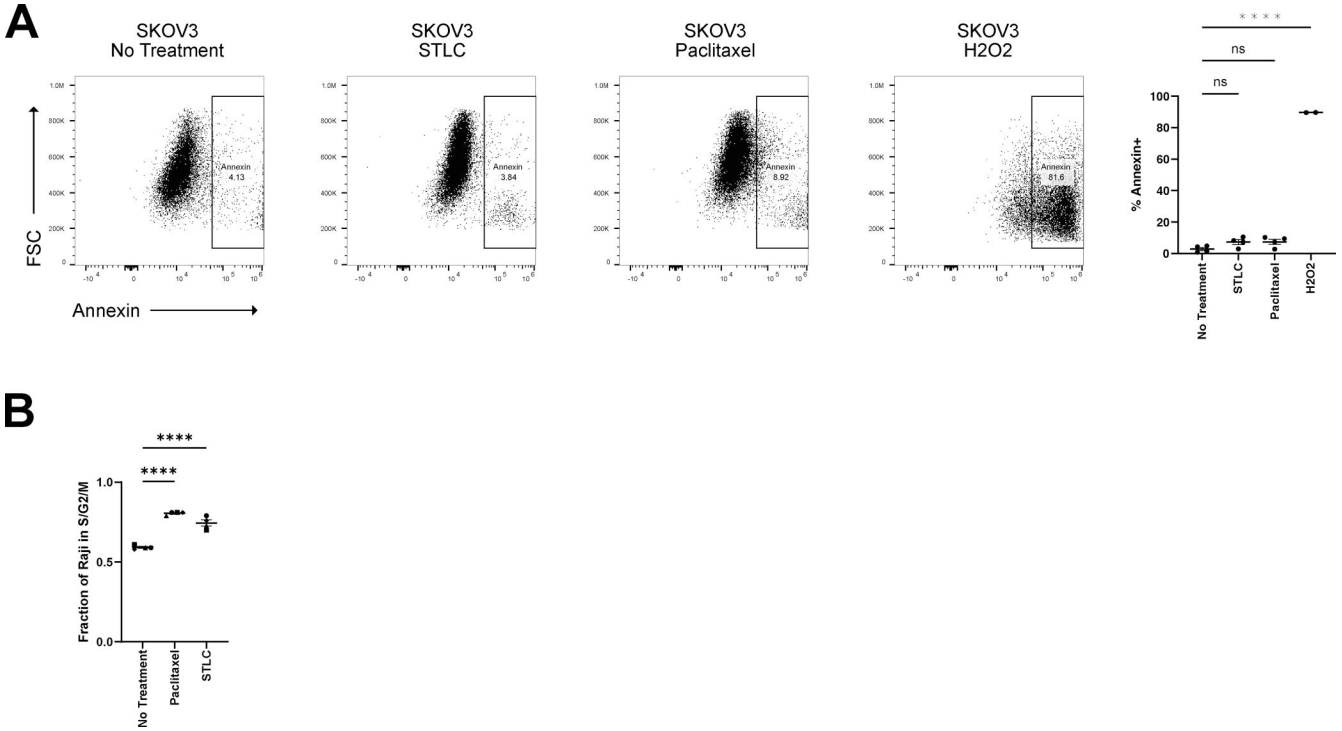

Figure S5. **Related to Fig. 7: STLC and paclitaxel do not cause widespread phosphatidylserine exposure after 24 h, and mitotic inhibitors increased the population of Raji cells in S/G2/M. (A)** SKOV3 cells were treated with STLC or paclitaxel for 20 h, then stained with annexin to measure phosphatidylserine exposure as an indicator of apoptosis. As a positive control, cells were treated with 250 µM H_2O_2 to induce apoptosis. Flow cytometry plots show a representative experiment. The graph depicts the percent of annexin-positive cells, with each dot representing an independent replicate. **(B)** FUCCI Raji cells were treated with STLC or paclitaxel for 20 h, then the samples were run in flow cytometry to verify mitotic inhibition. FUCCI Raji cells will appear mCh^+ when undergoing mitosis; however, this mCh^+ population is cumulative of S/G1/M. The mCh^+ population has been presented in this graph. Data in A and B were compared using one-way ANOVA with Holm–Sidak multiple comparison correction. *N* = 4 independent experiments. Bars represent the mean ± SEM. **** denotes P < 0.00005.

Video 1. **Her2 CAR macrophage phagocytosing an SKOV3 cell.** The video shows an Her2 CAR GFP (green) macrophage phagocytosing an SKOV3 cell (mCh-CAAX). Images were acquired on a spinning disc confocal every 4 min. Scale bar is 20 µm. Stills from this movie are shown in Fig. 1.

Video 2. **Her2 CAR macrophage trogocytosing an SKOV3 cell.** The video shows an Her2 CAR GFP (green) macrophage trogocytosing an SKOV3 cell (mCh-CAAX). Images were acquired on a spinning disc confocal every minute. Scale bar is 20 µm. Stills from this movie are shown in Fig. 1.

Video 3. **Her2 CAR macrophages infiltrate an SKOV3 spheroid.** The video moves through the z planes of an SKOV3 (mCherry-CAAX; magenta) incubated with Her2 CAR GFP (green) macrophages. The magenta line highlights the boundary of the spheroid in each slice. Scale bar denotes 40 µm. Images of a live, unfixed sample were acquired on a spinning disc confocal 24 h after the sample was encapsulated in Matrigel with macrophages. The distance between z slices is 10 µm, and the total depth is 120 µm.

Video 4. **GFP-CAAX macrophages infiltrate an SKOV3 spheroid.** The video moves through the z planes of an SKOV3 (mCherry-CAAX; magenta) incubated with GFP-CAAX (green) macrophages. The magenta line highlights the boundary of the spheroid in each slice. Scale bar denotes 40 µm. Images of a live, unfixed sample were acquired on a spinning disc confocal 24 h after the sample was encapsulated in Matrigel with macrophages. The distance between z slices is 10 µm, and the total depth is 120 µm.

Video 5. **Her2 CAR macrophage phagocytosing an SKOV3 cell in 3D spheroid.** The video shows an Her2 CAR GFP (green) macrophage phagocytosing an SKOV3 cell (mCh-CAAX) in a 3D spheroid. Images were acquired on a spinning disc confocal every 6 min. Scale bar is 20 µm. Stills from this movie are shown in Fig. S2.

Video 6. **Her2 CAR macrophage phagocytosing a dividing SKOV3 cell.** The video shows an Her2 CAR GFP (green) macrophage phagocytosing an dividing SKOV3 cell (mCh-CAAX). Images were acquired on a spinning disc confocal every minute. Scale bar is 20 µm. Stills from this movie are shown in Fig. 7.

Provided online are Table S1 and Data S1. Table S1 shows the sgRNA focal adhesion components. Data S1 shows Source data for Fig. 2 B.

Downloaded from http://rupress.org/jcb/article-pdf/224/11/e202502034/1950889/jcb_202502034.pdf by guest on 12 May 2026